

N71-35150
NASA OR-121874

CASE FILE
COPY



CENTER FOR SPACE RESEARCH
MASSACHUSETTS INSTITUTE OF TECHNOLOGY



00035

Massachusetts Institute of Technology
Center for Space Research

Thermal Control
for Mobile Packages
in the
Dusty Lunar Environment

TR 71-2

June 1971

by

Richard H. Baker
Richard J. Langley

ABSTRACT

Passive thermal protection concepts are developed to improve the thermal performance of simple radiative surfaces in mobile, dusty, lunar environments. The concepts consist of secondary surfaces which shade the primary surface at high solar elevations, thus, lowering the maximum temperatures incurred. At low solar elevations, the secondary blocks radiation from the primary surface and thereby raises its minimum temperature. Optimization parameters for dual surface configurations are illustrated.

Several methods of raising the minimum temperature of the primary surface at low solar elevations are discussed including solar powered heaters, variable area primary surfaces, glass covered high absorptance materials, and conical secondaries. Various means of lowering the maximum temperatures incurred by the basic dual surface design are described including multi-characteristic materials, conical secondary surfaces, and infrared radiation shields.

ACKNOWLEDGEMENT

We wish to express our gratitude to the MIT Center for Space Research and the Scientific Investigators of the SEP Experiment for affording us the opportunity to make this study.

SYMBOLS

- A_1 - area of the primary surface
- A_{1x} - unshaded area of the primary surface
- A_2 - area of the secondary surface
- A_{2B} - area of the bottom of the secondary surface
- A_{2T} - area of the top of the secondary surface
- A_{2x} - area of the secondary surface exposed to lunar albedo
- A_L - area of the lunar surface
- D_1 - diameter of the primary surface
- D_2 - diameter of the secondary surface
- F_{ij} - geometric view factor representing the fraction of energy radiated by surface i that is incident on surface j . Subscripts i and j follow the same definitions as those for area above
- G - solar constant
- H - height of the secondary surface
- H_p - height of the solar panel
- k_{ij} - ratio of area j to area i
- L - apparent displacement of two surface due to solar elevation
- P - internal power dissipation
- R_1 - radius of the primary surface
- R_2 - radius of the secondary surface
- R_{2B} - radius of the bottom of a conical secondary surface
- R_{2T} - radius of the top of a conical secondary surface
- α_s - solar absorptance, numerical subscripts refer to surface defined for areas

- β - angle between the side of a conical secondary and the horizontal
- ϵ - emittance, numerical subscripts refer to surfaces defined for areas
- σ - Stefan-Boltzman constant
- τ_V - transmittance in visible light spectrum
- τ_{IR} - transmittance in the infrared light spectrum
- θ - solar elevation

TABLE OF CONTENTS

	Page
1.0 Introduction	1
2.0 Fundamentals of Simple Radiative Surfaces	4
3.0 Planar Dual Surface Systems	10
3.1 General	10
3.2 Rachinonal for the Dual Surface Concept	10
3.2.1 Low Solar Elevations	10
3.2.2 High Solar Elevations	15
3.2.2.1 Dirty Surface Conditions	15
3.2.2.2 Super-Clean Surface Conditions	16
3.2.3 Summary	20
3.3 Dual Surface Performance	20
3.3.1 Assumptions for Equations	20
3.3.2 Thermal Equilibrium Equations	21
3.3.3 Typical Dual Surface Configuration	24
3.3.4 Observations	24
3.3.5 P/A Parameter for the Dual Surface Concept	26
3.3.6 Optimization of Parameters S/D_1 and D_2/D_1	28
3.4 Multi-Secondary Configurations	33
4.0 Conical Secondary Surfaces	37
4.1 Introduction	37
4.2 Analytic Development, High Solar Elevations	37
4.3 Generalized Thermal Equilibrium Equations	43
4.4 Computer Analysis	45
4.4.1 Cylindrical Secondaries	45
4.4.2 Conical Secondaries	46
4.4.3 Optimum Conical Secondary	47
5.0 Extensions	50
5.1 Solar Powered Heater	50
5.2 Variable Area Systems	55
5.3 Multi-Characteristic Dual Surface Configurations	57
5.4 Glass Surfaces	59

TABLE OF CONTENTS

(continued)

	Page
6.0 Conclusions and Recommendations	63
Appendix A	65
Appendix B	70
References	76

LIST OF FIGURES

	Page
Figure 1.1	3
Figure 2.1	5
2.2A	6
2.2B	7
2.3	9
Figure 3.1	11
3.2	13
3.3	13
3.4	14
3.5	14
3.6	14
3.7	19
3.8	19
3.9	19
3.10	25
3.11	27
3.12	29
3.13	29
3.14	31
3.15	32
3.16	34
3.17	34
3.18	36
Figure 4.1	38
4.2	38
4.3	38
4.4	40
4.5	40
4.6	48
Figure 5.1	52
5.2	54
5.3	56
5.4	58
5.5	58
5.6	58
5.7	60
5.8	60

1.0 INTRODUCTION

The concepts of thermal protection developed in this report are the results of work relating to the design of a thermal protection system for the Surface Electrical Properties (SEP) experiment scheduled to be flown as part of the Apollo 17 mission in 1972.

The SEP experiment is essentially a depth sounding concept and includes a stationary transmitter and a mobile receiver carried on the Lunar Rover Vehicle (LRV). Several techniques have been developed to adequately protect stationary electronic equipment in the harsh lunar environment which ranges from -175°C at lunar night through -60°C at dawn to $+125^{\circ}\text{C}$ at noon. However, the thermal protection of mobile equipment is complicated not only by the changing solar orientation but also lunar dust which degrades radiative surfaces. Further, the SEP receiver which dissipates about 6.5 watts internally includes a tape recorder which requires that the package internal temperature be held between $+5^{\circ}\text{C}$ and 50°C .

A large "thermal mass" using wax in a totally insulated envelope can and has been used; however, this technique necessarily requires a relative large mass and limits the duration of continuous operation. This report discusses various configurations and techniques which minimizes the effects of both variable solar orientation and lunar dust.

The NASA Manned Space Center has some preliminary information about how the radiative properties of various materials change with

dust cover and the results indicate that degradation of radiative surfaces causes the solar absorptance and the emittance to change and ultimately approach the values of the lunar surface ($\alpha_s = .90$, $\epsilon = .85$). In the report, second surface mirrors are used for the radiative surfaces which will be assumed to degrade with dust according to the description values given in Table 1.1. It should be noted that if surfaces other than second surface mirrors are used and the results, configurations, etc., report here are, in general, applicable.

Table 1.1

Clean and Degraded Values used
for Second Surface Mirrors

Contamination	α_s	ϵ
none (clean)	.085	.85
dusty	.20	.85
very dusty	.40	.85
dirty	.90	.85

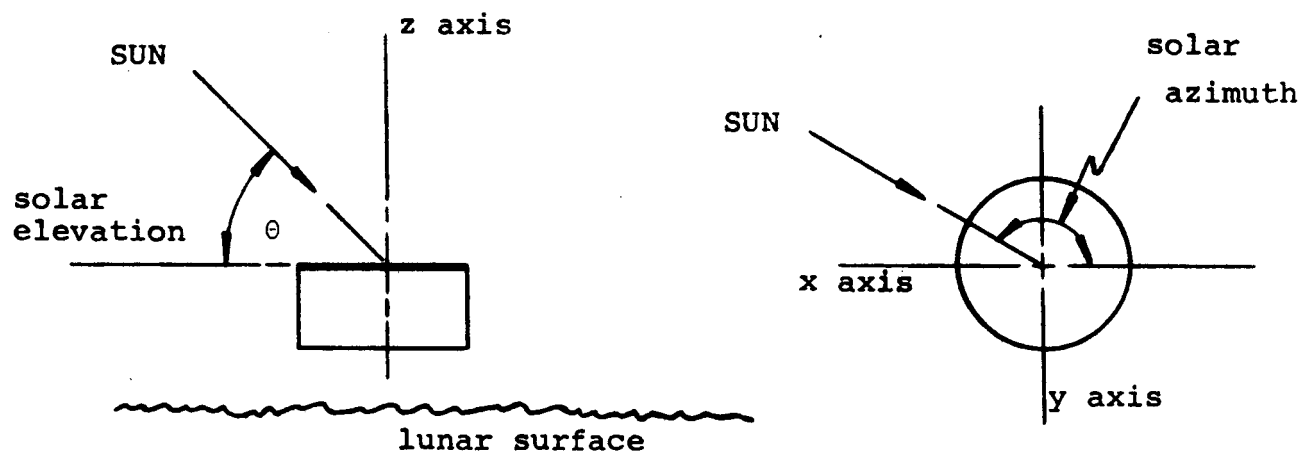


Figure 1.1
Azimuth and Elevation

2.0 FUNDAMENTALS OF SIMPLE RADIATIVE SURFACES

2.1 Equilibrium Equations

A basic thermal model for an experiment dissipating power through a radiative surface is shown in Figure 2.1. The equilibrium equation for this configuration may be written as:

$$\begin{array}{r} \left[\text{energy} \right] \\ \left[\text{radiated} \right] \end{array} = \begin{array}{r} \left[\text{internal power} \right] \\ \left[\text{dissipation} \right] \end{array} + \begin{array}{r} \left[\text{solar energy} \right] \\ \left[\text{absorbed} \right] \end{array}$$

$$\sigma \epsilon T^4 A = P + G \alpha_s A \sin (\theta) \quad (2.1)$$

where G = solar flux (130 watts/ft²)

P = internal power dissipation (watts)

σ = Stefan-Boltzmann Constant ($.527 \times 10^{-8} \frac{\text{watts}}{\text{ft}^2 - (\text{°K})^4}$)

α_s = solar absorptance of radiative surface
(see Table 1.1)

ϵ = emittance of radiative surface (.85)

A = area of radiative surface (ft²)

θ = solar elevation

T = equilibrium temperature of radiative surface (°K)

2.2 Performance of Simple Radiative Surface and Comparison to Requirements

From Equation 2.1, the temperature of the radiating surface of the basic model as a function of sun elevation and surface conditions for two different ratios of P/A is shown in Figures 2.2A and 2.2B.

Because the tape recorder limits the minimum and maximum allowable temperature for the SEP receiver to 5°C and 50°C

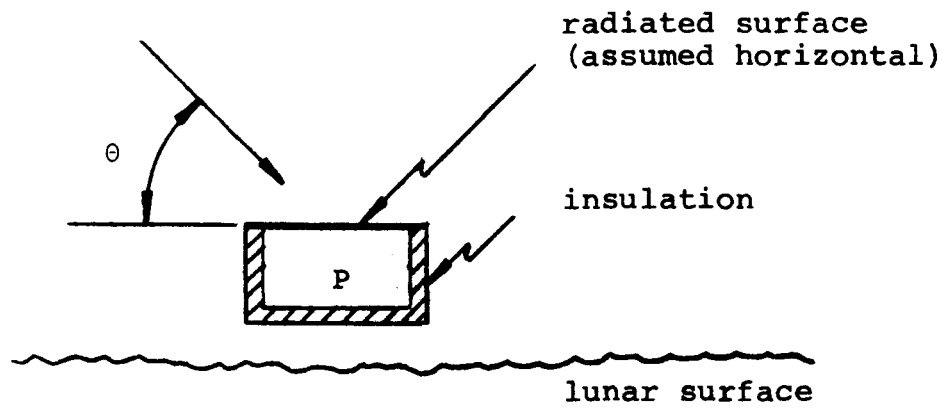


Figure 2.1

Basic Model for Lunar Experiment
with Simple Radiative Surface

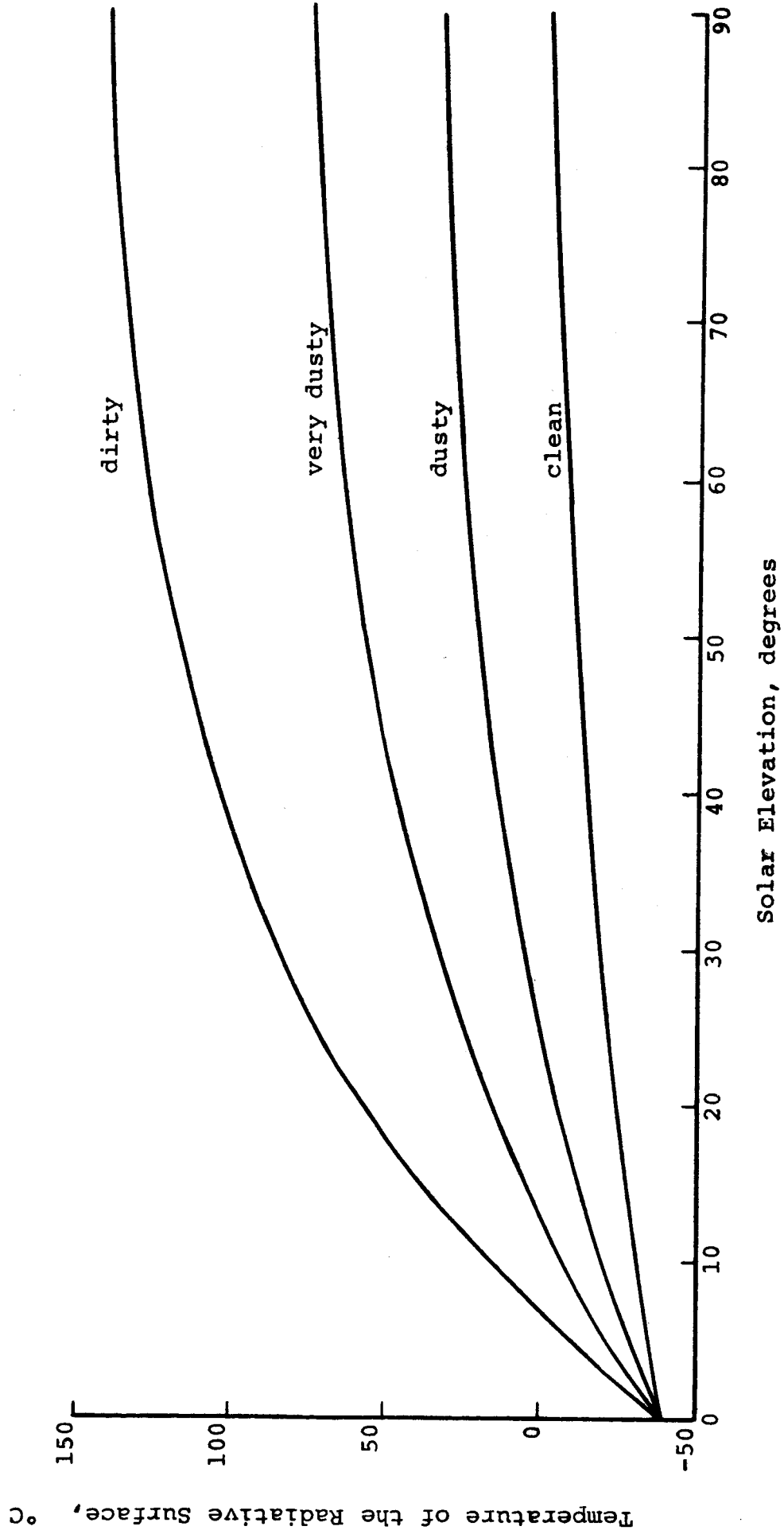
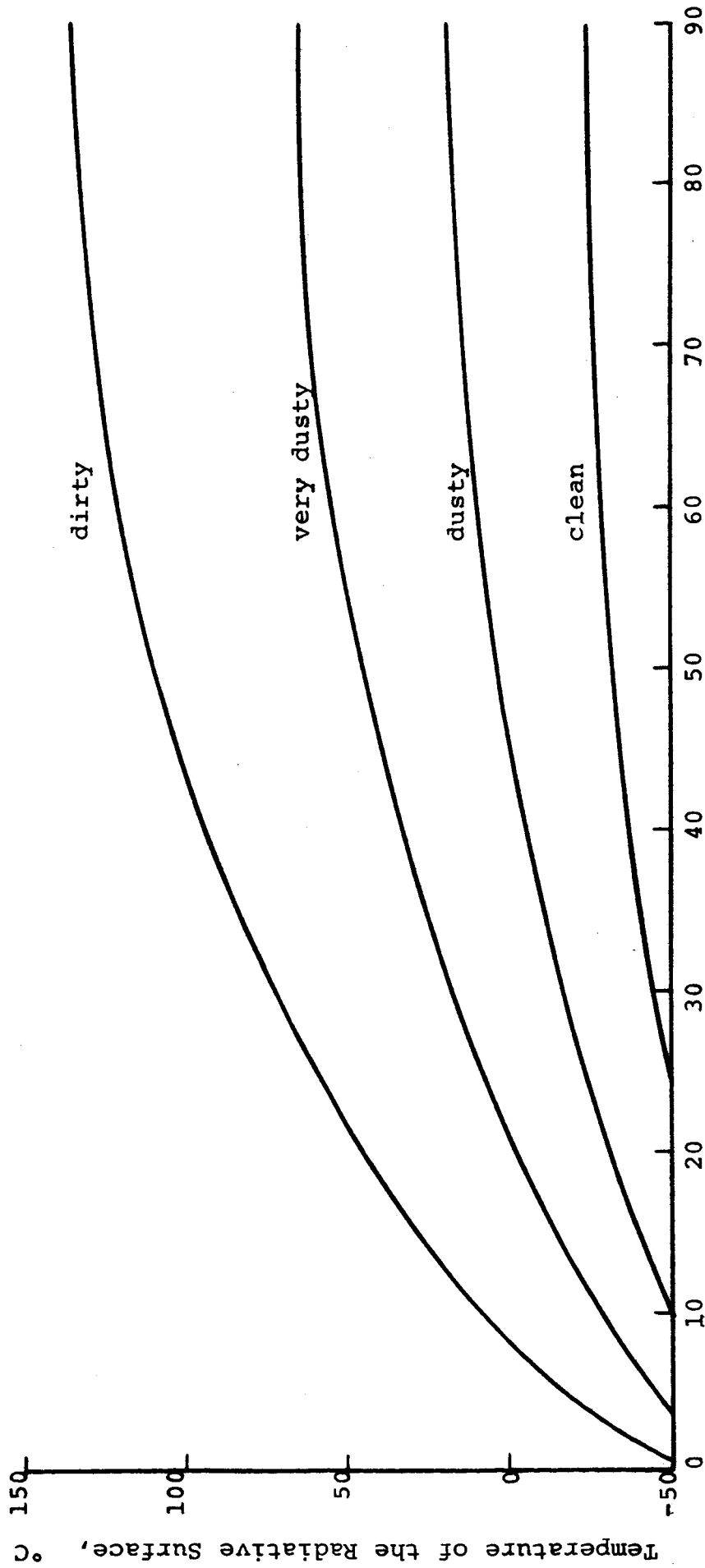


Figure 2.2A
 P/A = 13 watt/ft²
 Figure 2.2

Thermal Performance of Single Radiative Surface Model



Solar Elevation, degrees
 Figure 2.2B ~ P/A = 6.5 watt/ft²

respectively, the results of Figures 2.2A and 2.2B indicate that in order to meet the thermal requirements, it is necessary, as indicated qualitatively in Figure 2.3, to both raise the temperature at low sun elevations and lower it at high sun elevations. The following chapters develop concepts which achieve these goals.

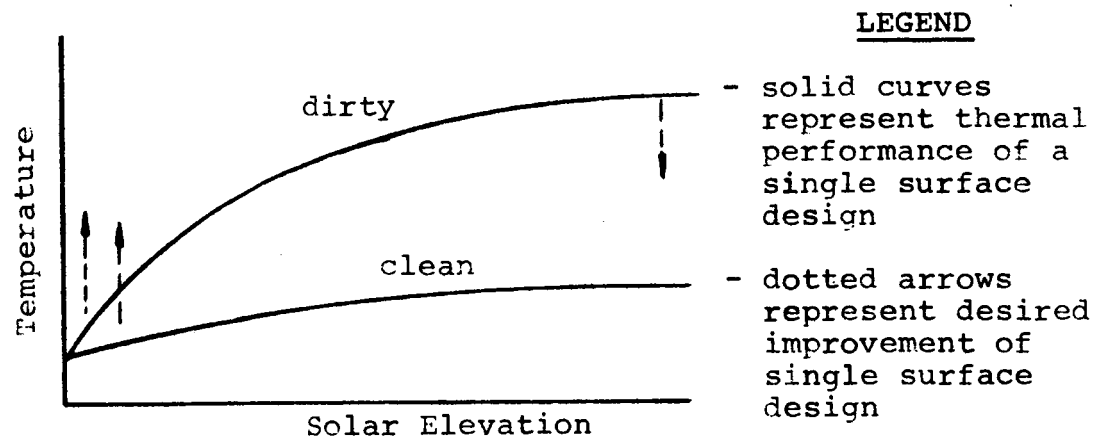


Figure 2.3

Thermal Performance of Basic Simple
Surface Model with Desired Improvements

3.0 PLANAR DUAL SURFACE SYSTEMS

3.1 General

A planar dual surface configuration will improve the thermal performance of the simple single radiative surface model of Figure 2.1. The basic configuration for the dual surface design consists of two parallel flat surfaces as shown in Figure 3.1. In this section, only flat plate secondary surfaces are discussed while Section 4.0 considers more complex secondary geometries.

3.2 Rachinonal for the Dual Surface Concept

A comparison of performance between the single and dual surface configurations is made in order to determine the relative thermal performance of the two configurations at high and low sun elevations. The method used in this comparison is to instantaneously create a second surface above the original single surface and examine the energy transfer from both surfaces to the surrounding medium at the instant of transition. For convenience, the energy transfers for the primary surface are based on the assumption that the temperature of the secondary is initially at the same temperature as the primary surface (see Figure 3.2). The temperature of the secondary is then shown to be consistent with the thermal inequalities shown for the primary surface.

3.2.1 Low Solar Elevations - Consider a single radiative surface (Figure 2.1) at zero degrees solar elevation. Solar energy is not incident on either the lunar surface or the radiating surface,

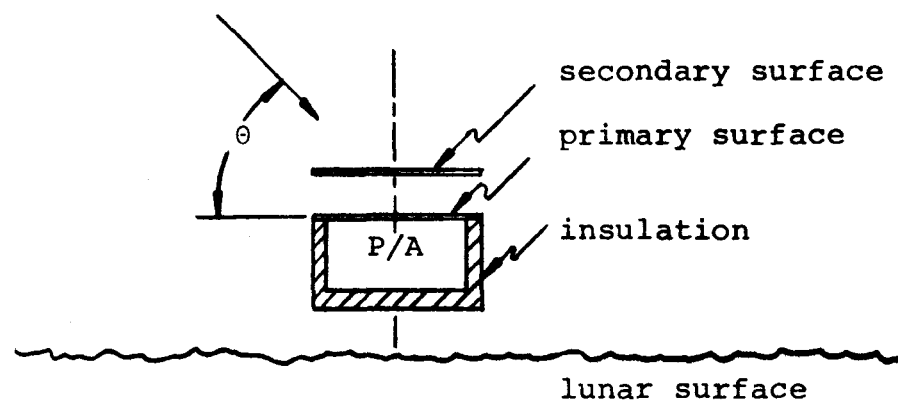


Figure 3.1

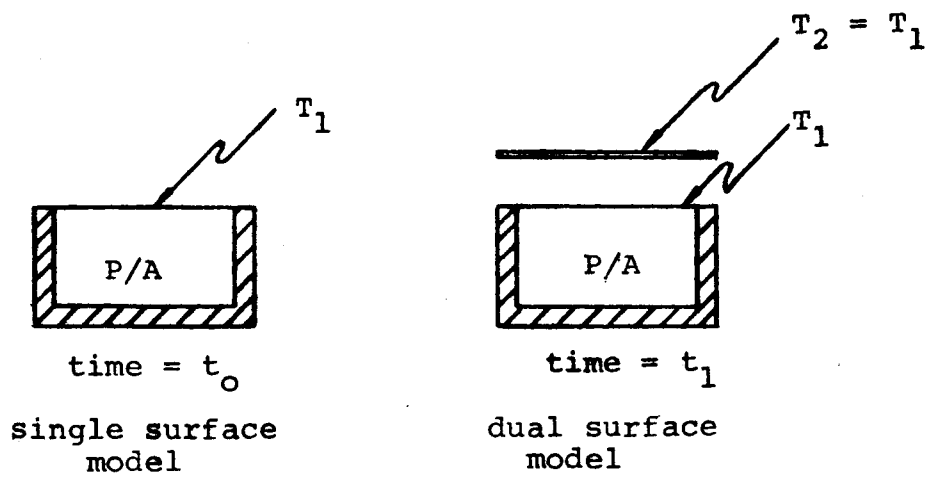
Basic Model for Lunar Experiment
with Dual Surface Configuration

thus, at this elevation the solar energy absorbed per unit time is independent of the surface degradation. Because the radiating surface is dissipating internal power, the radiating surface equilibrium temperature (T_1) is greater than that of the surrounding lunar surface (T_L).

The energy transfers for a dual surface configuration at time t_1 are shown in Figure 3.3. Now referring to Figures 3.2 and 3.3, it is known that $q_a = q_c + q_d$ at time t_0 because there is no absorption of solar energy. At time t_1 , the primary surface of the dual surface model radiates the same quantity of energy since it is still at temperature T_1 . There are only four components of energy transfer for the primary surface: q_a , q_b , q_c , and q_d . It is known that at time t_0 , $q_a = q_c + q_d$ and that $q_b > 0$. Thus, the inequality $q_a + q_b > q_c + q_d$ follows and, therefore, the primary surface absorbs more energy than it is emitting. Thus, temperature of the primary surface must increase (heat) in reaching a new equilibrium (for any finite temperature of the secondary surface).

For the secondary surface $q_e = q_f$ since $T_1 = T_2$ at time t_1 . Also, as noted previously, $T_2 > T_L$ and, hence, $q_g > q_h$. In addition $q_i > 0$ and, therefore, a net energy transfer to space and the lunar surface must occur. Accordingly, the secondary must cool in reaching a new equilibrium.

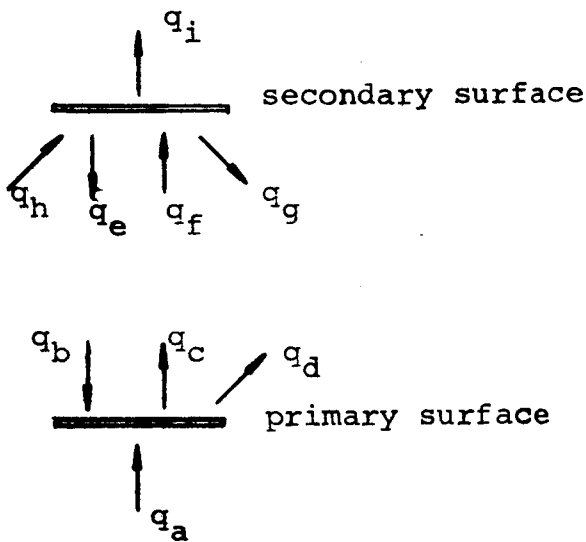
The net energy transfer for primary and secondary surfaces at time t_1 with zero degree solar elevation are shown in Figure 3.4.



$t_1 - t_0 \rightarrow 0$

Figure 3.2

Instantaneous Transition from Single Surface to Dual Surface Model



- q_a = internal power dissipation
- q_b = infrared radiation (IR) absorbed from secondary
- q_c = IR radiated to secondary
- q_d = IR radiated to space
- q_e = IR radiated to primary
- q_f = IR radiated from primary
- q_g = IR radiated to lunar surface
- q_h = IR absorbed from lunar surface
- q_i = IR radiated to space

Figure 3.3

Energy Transfers for Dual Surface Model at Instant of Transition

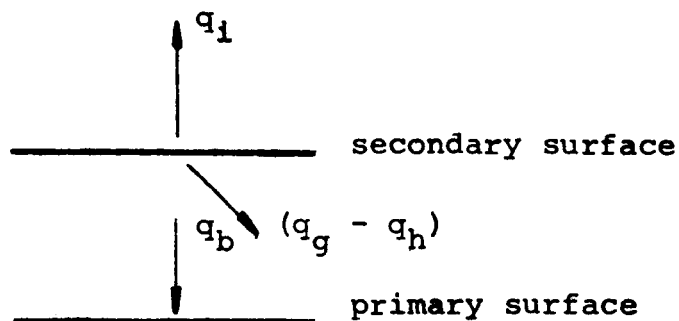


Figure 3.4

Net Energy Transfers for Dual Surface Model
at Time t_1 , Zero Degree Solar Elevation

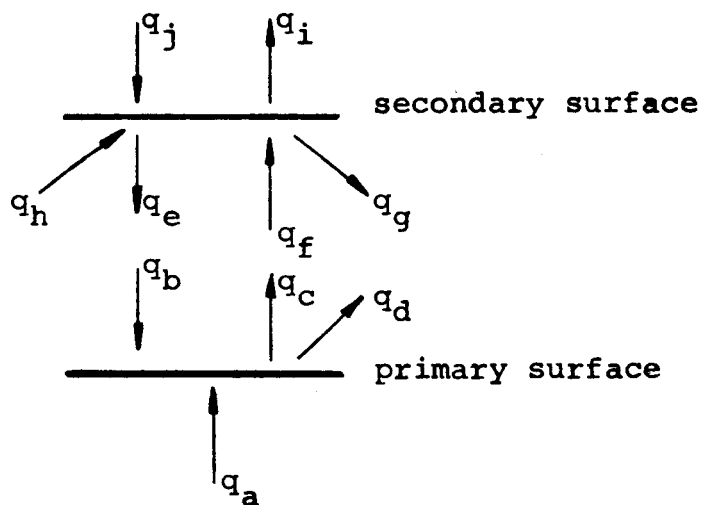


Figure 3.5
Energy Transfers for Dual Surface
Model at Time t_1 , Dirty Conditions

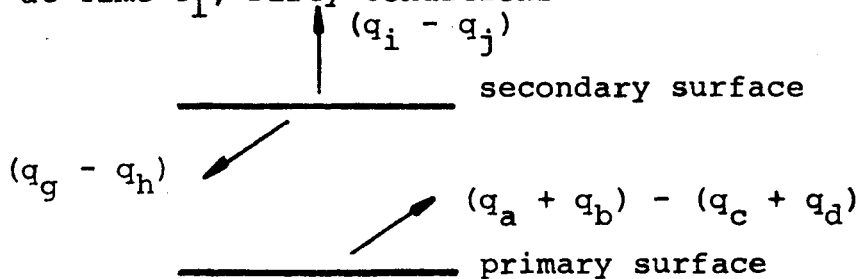


Figure 3.6

Net Energy Transfers for Dual
Surface Model, Dirty Conditions

3.2.2 High Solar Elevations - The radiative surfaces of both the single surface and dual surface models absorb solar energy at high sun elevations and in this section we consider the two limiting cases of solar absorptance for these surfaces; the is, (1) completely contaminated surfaces with high solar absorptance, and (2) clean surfaces with low solar absorptance.

3.2.2.1 Dirty Surface Conditions - Again, consider the instantaneous transition from a single surface into a dual surface model. Under dirty conditions, we assume that the single surface characteristics are identical to the lunar surface and since $P/A > 0$, we know that at the transition time t_1 , $T_1 = T_2 > T_L$. Figure 3.5 shows the energy transfers for both surfaces at time t_1 where q_a through q_i are defined as in Figure 3.3 and q_j is the solar energy absorbed by the secondary.

Considering the primary surface of Figure 3.5, if the separation of the surfaces approaches zero then $q_d \rightarrow 0$ such that q_c becomes the total emitted energy from the primary and q_b equals the solar absorption which is consistent with a single surface where the separation is equal to zero and the equilibrium equation is

$$q_a + q_b = q_c + q_d \text{ (where } q_d = 0\text{)}$$

As the separation distance is increased, q_d becomes larger; i.e., the primary "sees" more 3°K space and in addition, q_b becomes smaller because some of the emitted energy from the secondary is no longer incident on the primary surface. (Note that the above is true only if the temperature of the secondary does not increase

after separation to compensate for the decreased coupling of the two surfaces. The following paragraph demonstrates that the secondary actually cools.) With q_d and q_b decreasing with increasing separation then we know that

$$(q_a + q_b < q_c + q_d) \text{ or}$$

the energy absorbed is less than the energy emitted at time t_1 and the primary must cool in reaching a new equilibrium.

For the secondary surface at the instant of transition (Figure 3.5) $q_e = q_f$ because $T_1 = T_2$, and $q_h < q_g$ since $T_2 > T_L$. It can be shown that $q_i > q_j$ by examining the equilibrium condition for the single surface:

$$\begin{aligned} \left[\begin{array}{c} \text{energy} \\ \text{radiated} \end{array} \right] &= \left[\begin{array}{c} \text{solar energy} \\ \text{absorbed} \end{array} \right] + \left[\begin{array}{c} \text{internal power} \\ \text{dissipation} \end{array} \right] \\ q_i &= q_j + q_a \quad (3.3.2.1) \end{aligned}$$

Thus, $q_i > q_j$ for $P/A > 0$. At the instant of transition, there is a net energy transfer to space and the lunar surface, thus, the secondary must cool in reaching a new equilibrium.

The net energy transfers for primary and secondary surfaces at the time of transition are shown in Figure 3.6

3.2.2.2 Super-Clean Surface Conditions - Although in this report the minimum $\frac{\alpha}{\epsilon}$ ratio is assumed to be .10, it is convenient for purposes of conceptually developing the dual surface model to define a "super-clean" surface with $\frac{\alpha_s}{\epsilon} = 0$. Such a surface absorbs no solar energy ($\alpha_s = 0$) but does absorb IR radiation ($\epsilon = .85$) and, therefore, the equilibrium of the single surface model will depend solely on the P/A ratio. In principal any desired temperature may be achieved by increasing or decreasing

the area of the radiative surface of the model but here where the object is to protect the electronic components from excessive temperatures less than the 125°C lunar surface. At $\theta = 90^\circ$, then $T_1 < T_L$. Energy transfers for primary and secondary surfaces were defined as in Figure 3.5. The only difference between the analysis of super-clean and dirty surfaces is that because there is no solar absorptance and there is internal power dissipation then $T_1 < T_L$.

For the primary surface of the dual surface model, we know that $q_a = q_c + q_d$ (no absorption of solar energy) and since $q_b > 0$, there is a net energy transfer into the primary and; accordingly, the primary surface must heat in reaching a new equilibrium.

For the secondary surface $q_j = 0$ and $q_e = q_f$. Because $T_2 < T_L$, $q_g < q_h$. Also, $q_i > 0$. The quantity $(q_h - q_g)$ is dependent on the separation of the plates and the temperature T_2 . Since T_2 is dependent solely on P/A , the change in secondary surface temperature is dependent on separation and P/A .

Mathematically,

$$q_i = \sigma \epsilon_2 T_2^4 A_2 = P \text{ (single surface equilibrium equation) } \quad (3.1)$$

$$\text{and } (q_h - q_g) = \sigma \epsilon_L (T_L^4 - T_2^4) F_{2L} A_2 \epsilon_2 \quad (3.2)$$

where ϵ_L = emittance of lunar surface (.85)

ϵ_2 = emittance of secondary surface ($\epsilon_2 = \epsilon_L$)

T_2 = temperature of secondary surface

T_L = temperature of lunar surface

A_2 = area of secondary surface

F_{2L} = geometric view factor representing fraction of energy emitted from secondary that is incident on lunar surface

Assuming that the lunar surface temperature may be approximated by

$$T_L = 4 \sqrt{\frac{G\alpha_L \sin(\theta)}{\sigma \epsilon_L}} \quad (3.2.2)$$

where α_L is the solar absorptance of the lunar surface then

$$(q_h - q_g) = (G\alpha_L - P/A)F_{2L}A\epsilon_2 \quad (3.2.3)$$

The secondary heats for

$$q_i < (q_h - q_g) \text{ which may be rewritten using equations 3.1 and 3.2.}$$

$$P < (G\alpha_L - P/A)F_{2L}A\epsilon_2 \quad (3.2.4)$$

$$P/A < \frac{G\alpha_L F_{2L} \epsilon_2}{1 + F_{2L} \epsilon_2} \quad (3.3)$$

Equation 3.3 is true for small values of the ratio P/A provided the view factor F_{2L} does not approach zero. This condition is satisfied for all of the configurations discussed in this study. The following parameters typically apply to all configurations:

$$P/A = 6.5 \text{ wt/ft}^2$$

$$G = 130 \text{ wt/ft}^2$$

$$F_{2L} = .55$$

$$\epsilon_2 = \epsilon_L = .85$$

$$\alpha_L = .90$$

Substituting these values into Equation 3.3, results in the inequality $6.5 < 35$. Thus, the secondary would heat in reaching the new equilibrium.

The net energy transfers for primary and secondary surfaces at the instant of transition is shown in Figure 3.7.

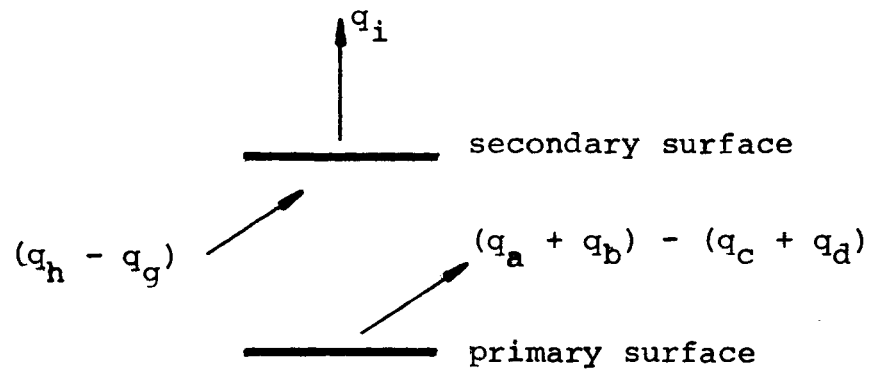


Figure 3.7

Net Energy Transfers for Dual Surface Model, Super-Clean Conditions

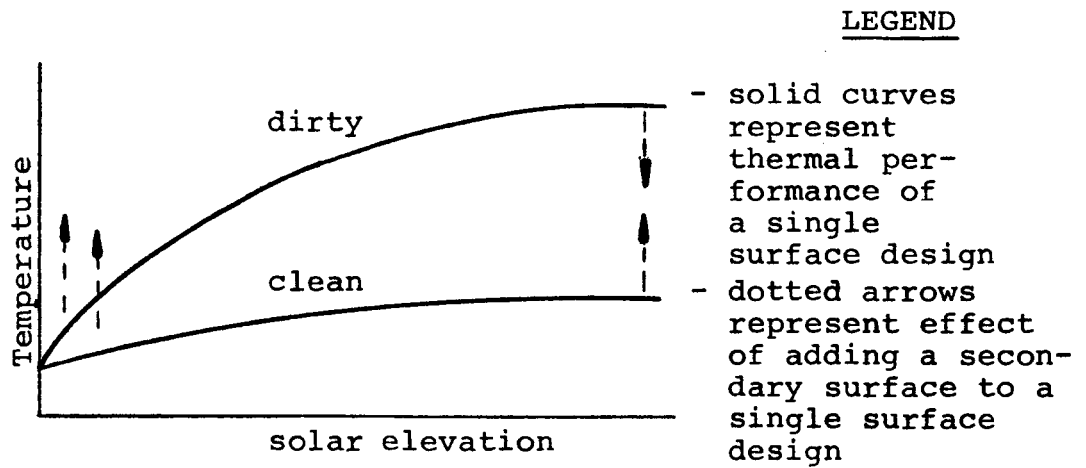


Figure 3.8

Qualitative Improvement of Dual Surface Model Relative to Single Surface Model

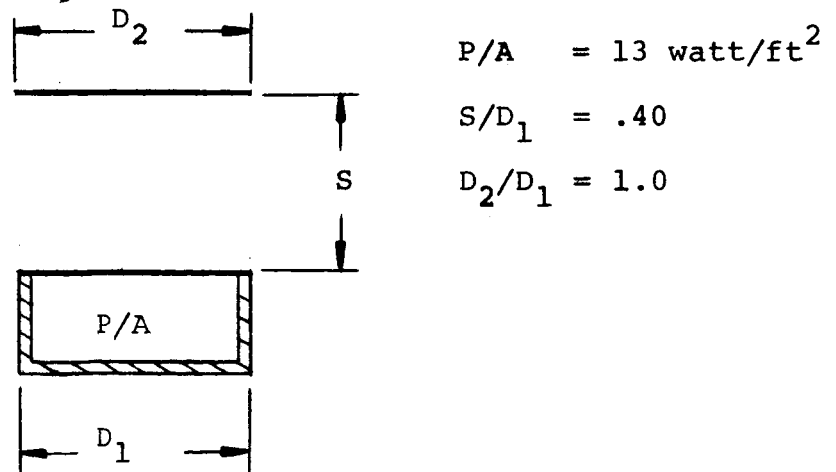


Figure 3.9

Basic Dual Surface Configuration, Example No. 1

3.2.3 Summary - At low sun elevations, the dual surface design raises the primary surface temperature relative to that of the single surface model. At high sun elevations, the dual surface design lowers the primary surface temperature for dirty conditions and raises the temperature for clean conditions relative to the single surface model. The qualitative result is indicated in Figure 3.8.

3.3 Dual Surface Performance

In this section the basic thermal equilibrium equations are developed and used to numerically demonstrate the thermal performance of the dual surface configuration.

3.3.1 Assumptions for Equations - Six assumptions are made in developing the equilibrium equations:

1. There is no energy transfer through the insulation on the sides and bottom of the experiment package.
2. All surfaces are isothermal.
3. All surfaces are diffuse (Lambert's Cosine Law).
4. Nearly all of the IR radiation is absorbed by the surface it is incident upon and a large fraction of the remainder is reflected away from the configuration. This is a good approximation because we are dealing with high emittance surfaces and geometric view factors in the configurations considered is generally less than unity.
5. Lunar albedo is diffuse. For computation purposes, albedo is included in the lunar IR term. This is acceptable because in the configurations to be considered, it yields a conservative estimate of thermal performance.

6. The primary radiative surface is assumed to remain level with respect to the lunar horizon and the lunar surface is assumed to be flat. This allows solar elevation to be measured relative to either the experiment package or the lunar horizon and the lunar surface temperature to be calculated as a simple function of solar elevation.

3.3.2 Thermal Equilibrium Equations - The equilibrium equations for the dual surface configuration of Figure 3.1 (page 11) may be written as follows:

Equilibrium of the primary surface:

$$\boxed{\text{energy radiated}} = \boxed{\text{solar energy absorbed}} + \boxed{\text{internal dissipation}} + \boxed{\text{secondary IR absorbed}} \quad (3.1)$$

$$\sigma \epsilon_1 A_1 T_1^4 = G \alpha_{s1} \sin(\theta) A_{1x} + P + \sigma \epsilon_2 A_2 F_{21} T_2^4 \epsilon_1 \quad (3.2)$$

Equilibrium of the secondary surface:

$$\begin{aligned} & \boxed{\text{energy radiated (both sides)}} = \boxed{\text{direct solar energy absorbed}} + \boxed{\text{solar energy reflected from primary surface}} \\ + & \boxed{\text{lunar albedo absorbed}} + \boxed{\text{lunar IR absorbed}} + \boxed{\text{IR from primary surface absorbed}} \quad (3.3) \end{aligned}$$

$$\begin{aligned} \sigma \epsilon_2 A_2 T_2^4 = & G \alpha_{s2} \sin(\theta) A_2 + G(1 - \alpha_{s1}) \sin(\theta) A_{1x} \\ & + G(1 - \alpha_L) \sin(\theta) A_{2x} + \sigma \epsilon_L A_L F_{L2} T_L^4 \epsilon_2 \\ & + \sigma \epsilon_1 A_1 F_{12} T_1^4 \epsilon_2 \quad (3.4) \end{aligned}$$

where A_{1x} = the unshaded area of the primary surface (see Appendix A).

A_{2x} = the area of the secondary exposed to lunar albedo (not used in numerical computations since albedo is included in lunar IR term).

F_{12} , F_{21} , and F_{2L} are geometric view factors calculated as follows (see Reference 4).

$$F_{12} = 1/2 (x - \sqrt{x^2 - 4E^2D^2}) \quad (3.5)$$

$$x = 1 + (1+E^2)D^2$$

$$D = 2S/D_1$$

$$E = D_2/(2S)$$

$$F_{21} = \frac{A_1}{A_2} F_{12} \quad (\text{Reciprocity Law for view factors}) \quad (3.6)$$

$$F_{2L} = 1 - F_{21} \quad (\text{Summation Law for view factors}) \quad (3.7)$$

Note that the view factors are explicit functions of the ratios S/D_1 and D_2/D_1 .

Equations 3.2 and 3.4 may be normalized by defining constants k_{12} , K_{1x} , and k_{2x} as follows:

$$\begin{aligned} A_2 &= k_{12}A_1 \\ A_{1x} &= k_{1x}A_1 \\ A_{2x} &= k_{2x}A_2 = k_{2x}k_{12}A_1 \end{aligned} \quad (3.8)$$

Also, the Reciprocity Law for view factors allows the following substitution to be made:

$$A_2F_{2L} = A_LF_{L2} \quad (3.9)$$

Substituting equations 3.8 and 3.9 into equations 3.2 and 3.4 and dividing by A_1 , the only term involving area is the term P/A_1 in equation 3.2. All other terms contain only the "k" constants which are dependent on relative dimensions. The significance of this normalization is that the dual surface configuration may be scaled to any power level by increasing its size. Since the scaling term

is an area, linear dimensions of a particular design increase as the square root of the ratio of power levels. (For example, increasing the power level from 6.5 to 650 watts would require scaling the linear dimensions of the design by a factor of 10.)

The resultant normalized equations are:

$$\sigma \epsilon_1 T_1^4 = G \alpha_{s1} \sin(\theta) k_{1x} + P/A_1 + \sigma \epsilon_2 k_{12} F_{21} T_2^4 \epsilon_1 \quad (3.10)$$

$$\begin{aligned} \sigma \epsilon_2 k_{12} T_2^4 &= G \alpha_{s2} \sin(\theta) k_{12} + G(1-\alpha_{s2}) \sin(\theta) k_{1x} + \\ &G(1-\alpha_L) \sin(\theta) k_{12} k_{2x} + \sigma \epsilon_L k_{12} F_{2L} T_L^4 \epsilon_2 + \sigma \epsilon_1 F_{12} T_1^4 \epsilon_2 \end{aligned} \quad (3.11)$$

Equations 3.10 and 3.11 may be solved explicitly for the equilibrium temperature of the primary surface.

$$T_1 = \left[\frac{2}{\sigma \epsilon_1 (2 - F_{21} \epsilon_1 \sigma F_{12} \epsilon_2)} \left[G \alpha_{s1} \sin(\theta) k_{1x} + P/A + \frac{F_{12} \epsilon_1}{2} \left[G \alpha_{s2} \sin(\theta) k_{12} + G(1-\alpha_{s2}) \sin(\theta) k_{1x} + G(1-\alpha_L) \sin(\theta) k_{12} k_{2x} + \sigma \epsilon_L k_{12} F_{2L} T_L^4 \epsilon_2 \right] \right] \right]^{1/4} \quad (3.12)$$

Since the view factors are explicit functions of S/D_1 and D_2/D_1 , the temperature of the primary surface may be written as:

$$T_1 = T_1(P/A_1, S/D_1, D_2/D_1, z_1, z_2, \dots, z_n) \quad (3.13)$$

where z_1, z_2, \dots, z_n are constants containing G ,

α_s, ϵ , etc.

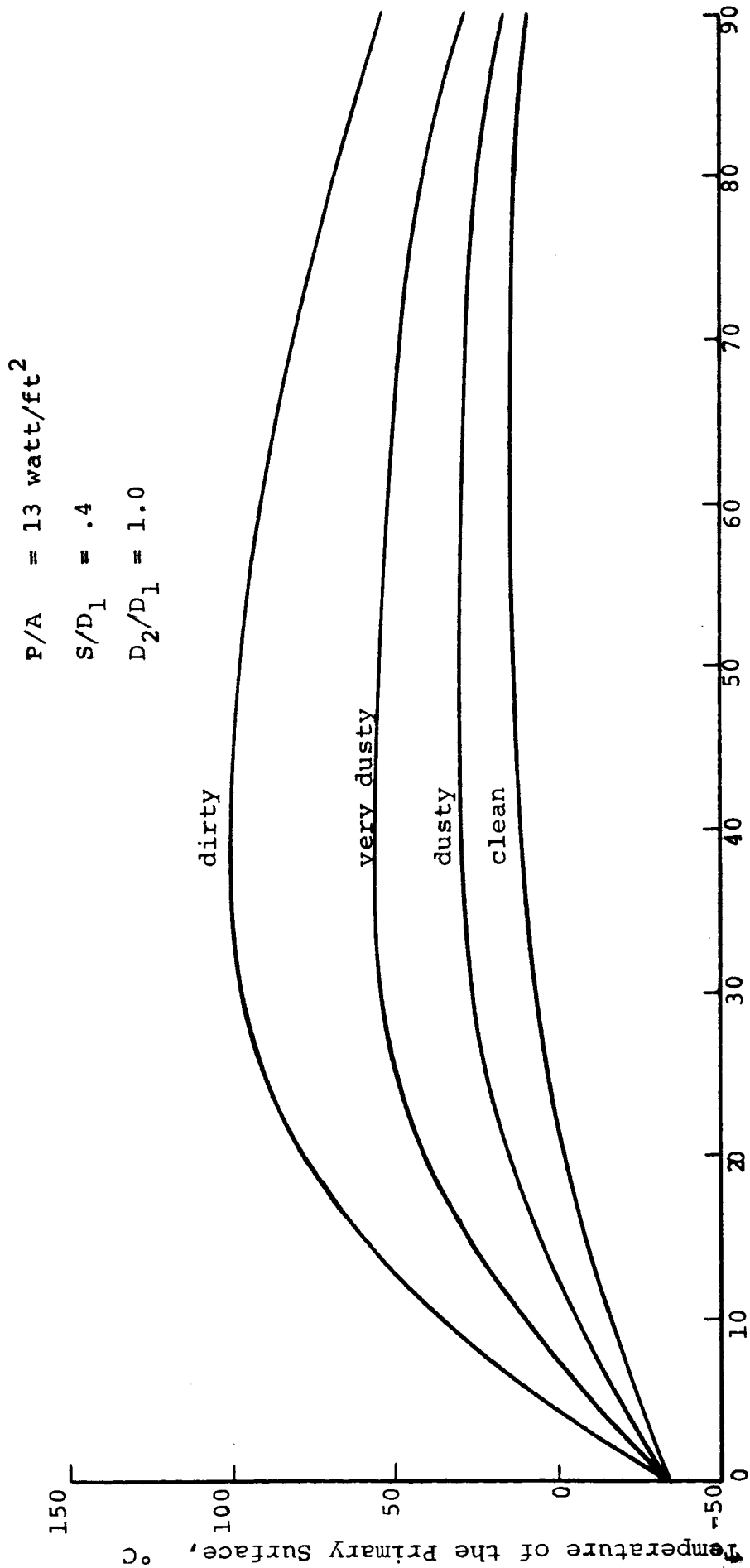
Equation 3.13 is used as the basis for subsequent discussion of optimization parameters for the dual surface configuration.

3.3.3 Typical Dual Surface Configuration - Before proceeding with the optimization of the dual surface design, it is informative to present two simple examples that demonstrate the thermal performance of typical configurations. The configuration for example No. 1, shown in Figure 3.9, represents an initial estimate of possible design parameters for the SEP receiver. The parameter $P/A = 13 \text{ watts/ft}^2$ represents a compromise between allowable physical size of the experiment package and required area to dissipate internal power. The separation parameter S/D_1 is large enough to reduce secondary IR absorbed by the primary surface but small enough to shade the primary at high solar elevations which result in excessive temperatures for unshaded surfaces. The parameter D_2/D_1 is set equal to unity for the first example.

The temperature of the primary surface for example No. 1 is plotted as a function of solar elevation and surface degradation in Figure 3.10.

3.3.4 Observations - Several important conclusions can be drawn from Figure 3.10.

1. The minimum temperature for the dual surface design is higher than for the single surface design (Figure 2.2A) but still falls below the minimum allowable temperature for the SEP receiver (5°C).
2. The maximum temperature does not occur at $\theta = 90^\circ$. Instead, the temperature of the primary surface actually decreases at high sun elevations because the secondary surface is providing more shade. The decrease in primary surface temperature at high solar elevations is limited by the fact that the secondary is absorbing more energy from the lunar surface and the sun. Some of this absorbed energy is reradiated to the primary surface partially compensating for the shading provided by the secondary.



Solar Elevation, degrees

Figure 3.10

Thermal Performance of Basic Dual Surface Configuration, Example No. 1

3. The primary surface temperature shows less sensitivity to dust degradation than for the single surface design. The temperature single surface design with $P/A = 13 \text{ wt/ft}^2$ fluctuated over a range of 143°C (at $\theta = 90^\circ$) due to dust degradation of the radiative surface. The primary surface in a dual surface design under identical circumstances varies only 55°C .
4. The maximum temperature of the primary surface in a dual surface design is lower than the maximum temperature for a single surface design. Actually, the maximum temperature for this example under very dusty conditions only exceeds the maximum allowable temperature for the SEP receiver (50°C) by 6°C .

3.3.5 P/A Parameter for the Dual Surface Concept - An extremely important parameter for radiative surface thermal protection systems is the value of the ratio P/A . The results of equation 3.12 may be reduced to an equation of the form

$$T_1 = 4 C_1 + C_2 (P/A_1) \quad (3.14)$$

where C_1 and C_2 are functions of constants other than P/A_1 . Therefore, for a given power level, increasing the area decreases temperatures at all sun elevations. As the area becomes very large, the increase in area has less and less effect and the thermal performance approaches that of a configuration with no internal power dissipation.

Example No. 2 demonstrates quantitatively the effect of changing the value of P/A by decreasing the value of P/A in example No. 1 to 6.5 watts/ft^2 . The temperature of the primary surface for example No. 2 is plotted in Figure 3.11 as a function of solar elevation and surface degradation.

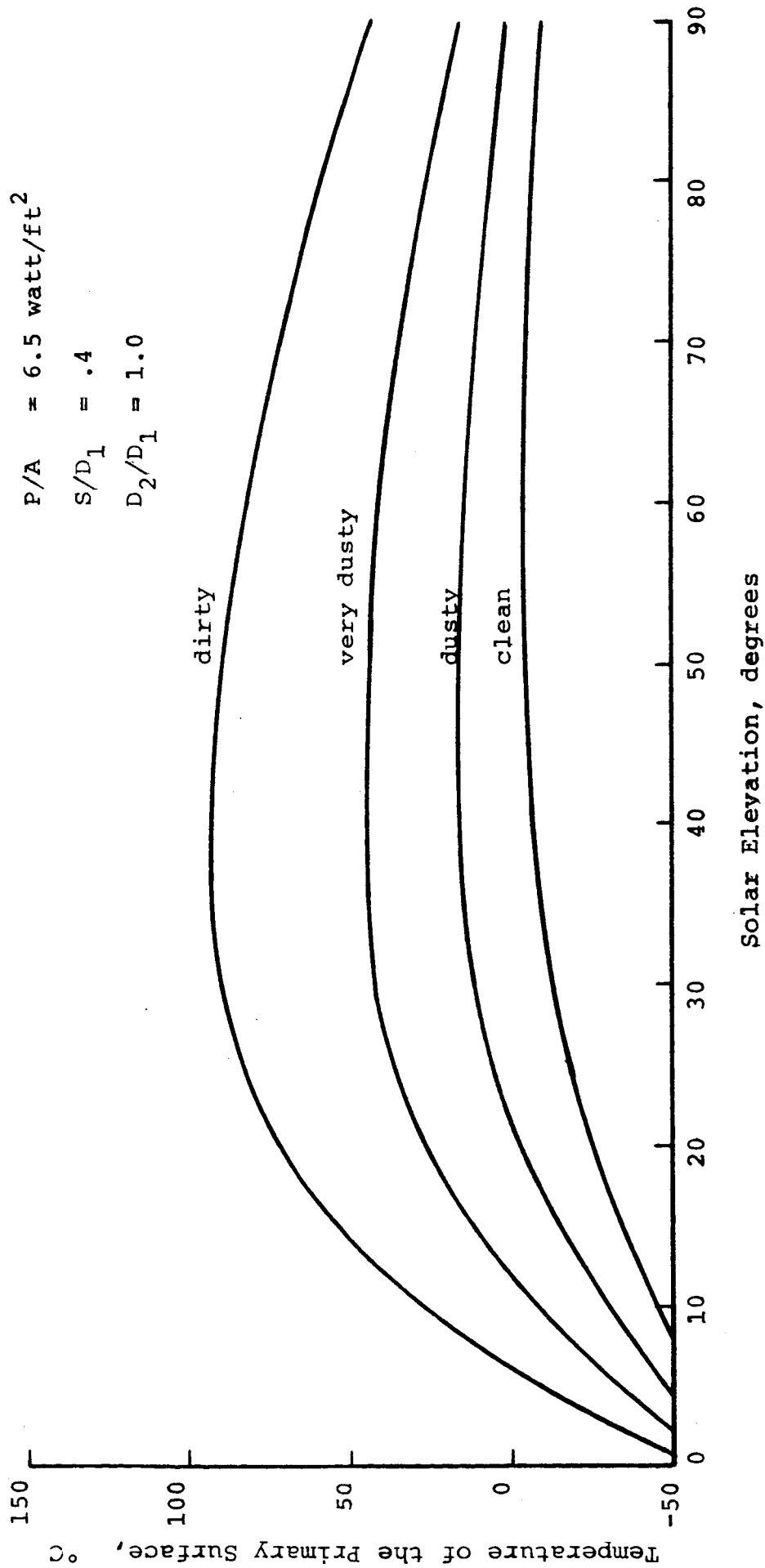


Figure 3.11

Thermal Performance of Basic Dual Surface Configuration with Modified Ratio of P/A, Example No. 2

Note that the minimum temperature of the primary surface decreased more than does the maximum temperatures. If the parameter P/A is used to decrease maximum temperatures, the physical size of the configuration must be increased and it becomes more difficult to maintain minimum operating temperatures at low solar elevations.

3.3.6 Optimization of Parameters S/D_1 and D_2/D_1 - The performance of the dual surface configuration may be improved by optimizing values for the parameters D_2/D_1 and S/D_1 . Figure 3.12 shows the relation of the minimum and maximum temperatures of the primary surface to the variable S/D_1 . The results were generated by iterating the parameter S/D_1 in equation 3.12 for all solar elevations and noting the minimum and maximum temperature for each iteration of the separation parameter. From Figure 3.12, the value $S/D_1 = .25$ yields the lowest maximum temperatures and highest minimum temperatures for $P/A = 13 \text{ watts/ft}^2$ and $D_2/D_1 = 1.0$. It is important to note that changing the parameter S/D_1 changes not only the maximum temperature incurred by the primary surface but also the solar elevation at which the maximum temperature will occur.

Figure 3.13 is generated in a manner similar to Figure 3.12 and shows the relation of minimum and maximum primary surface temperatures to the variable D_2/D_1 with $P/A = 13 \text{ watts/ft}^2$ and $S/D_1 = .25$. The parameter D_2/D_1 is not nearly as significant as the parameters P/A and S/D_1 as seen from the flatness of the curves

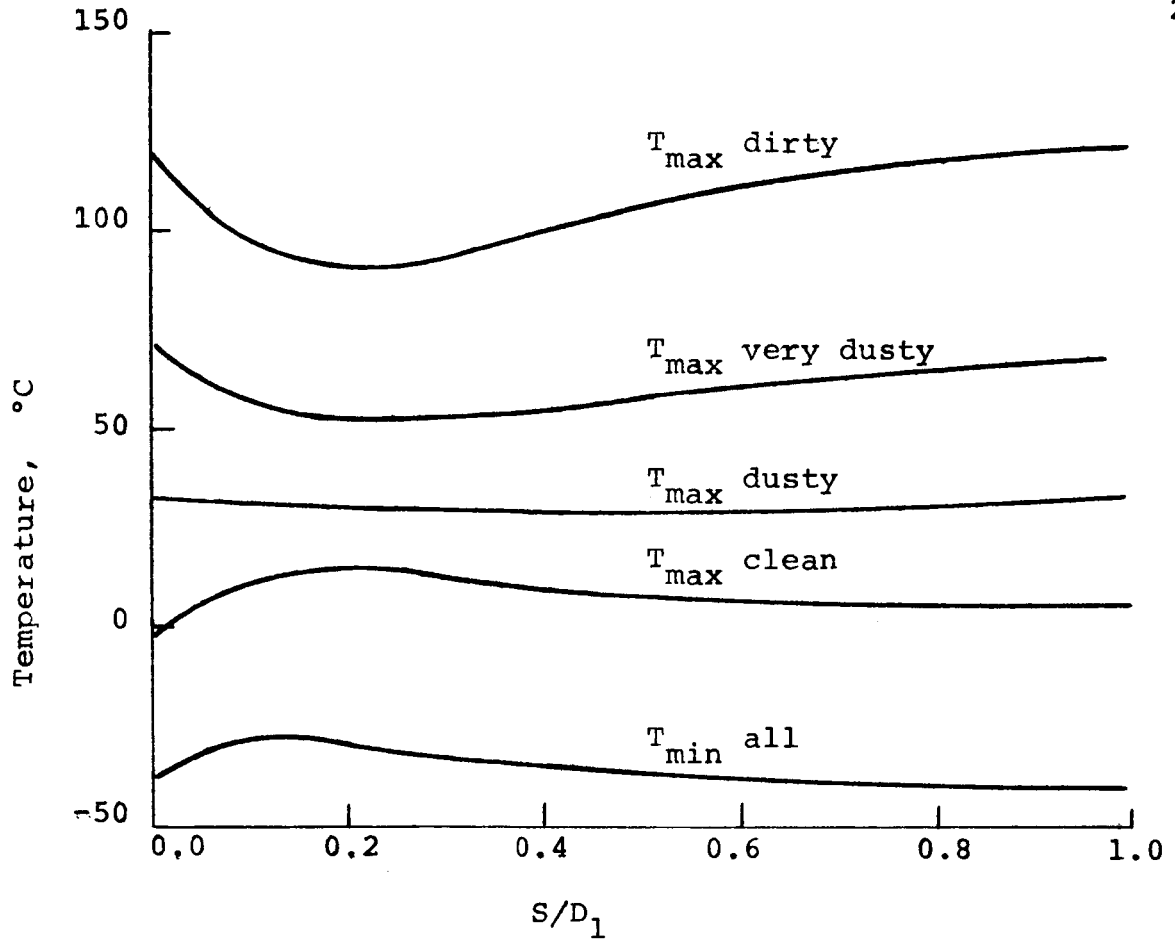


Figure 3.12
Optimization of S/D_1 Parameter

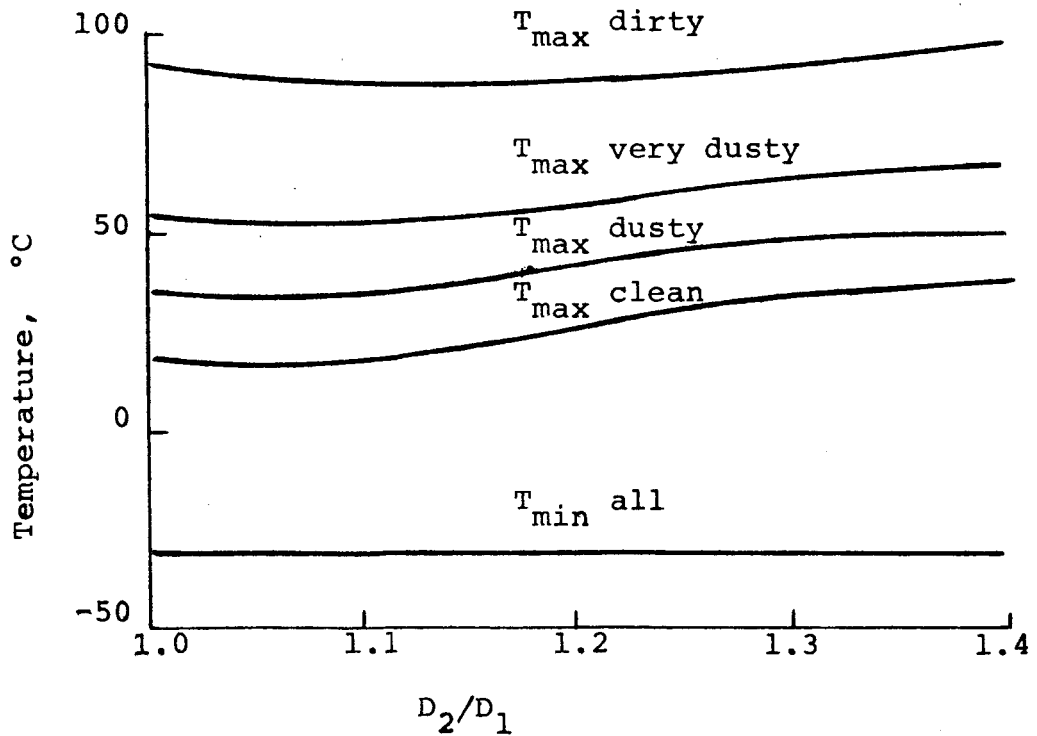


Figure 3.13
Optimization of D_2/D_1 Parameter

in Figure 3.13. A value of $D_2/D_1 = 1.1$ slightly improves the thermal performance of example No. 1 by lowering the maximum temperature by one or two degrees centigrade.

The chief significance of parameters S/D_1 and D_2/D_1 are that they effect the tradeoff between the amount of direct solar energy absorbed and reradiated IR energy. As the separation of the surfaces in a dual surface design is decreased, two effects tend to lower the temperature of the primary surface: i) the primary is more shaded from solar flux, and ii) the secondary absorbs less lunar IR. At the same time, however, the view factors F_{12} and F_{21} increase tending to raise the temperature of the primary surface. Conversely, if the separation is increased, the view factors are decreased and the primary surface is exposed to more solar energy. Increasing D_2/D_1 causes the primary surface to be shaded more quickly as the solar elevation changes as shown in Appendix A but it also allows the secondary to absorb more energy in the form of lunar IR and solar flux.

Example No. 3, which is shown in Figure 3.14, incorporates the results of Figures 3.12 and 3.13 and represents an optimum design for the planar dual surface design. The thermal performance of example No. 3 is plotted in Figure 3.15. The effects of optimization may be seen by comparing the thermal performance of example No. 1 and example No. 3 (Figures 3.10 and 3.15). The maximum temperatures have been lowered and the temperatures at very high sun elevations have been raised slightly. The result is a flattening of the thermal curves with a resultant lower maximum temperature and higher minimum temperature.

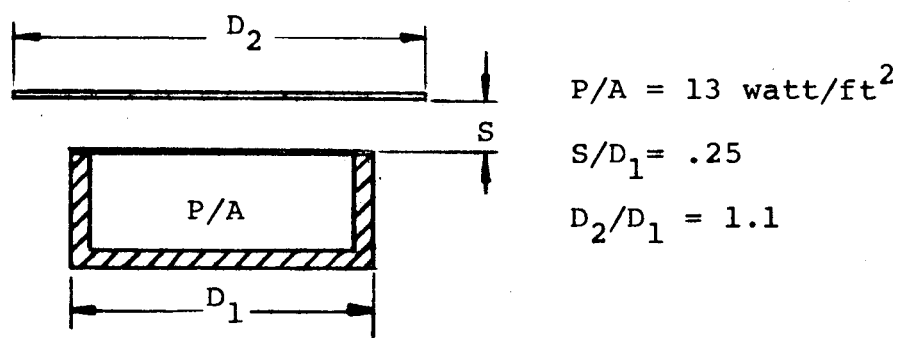
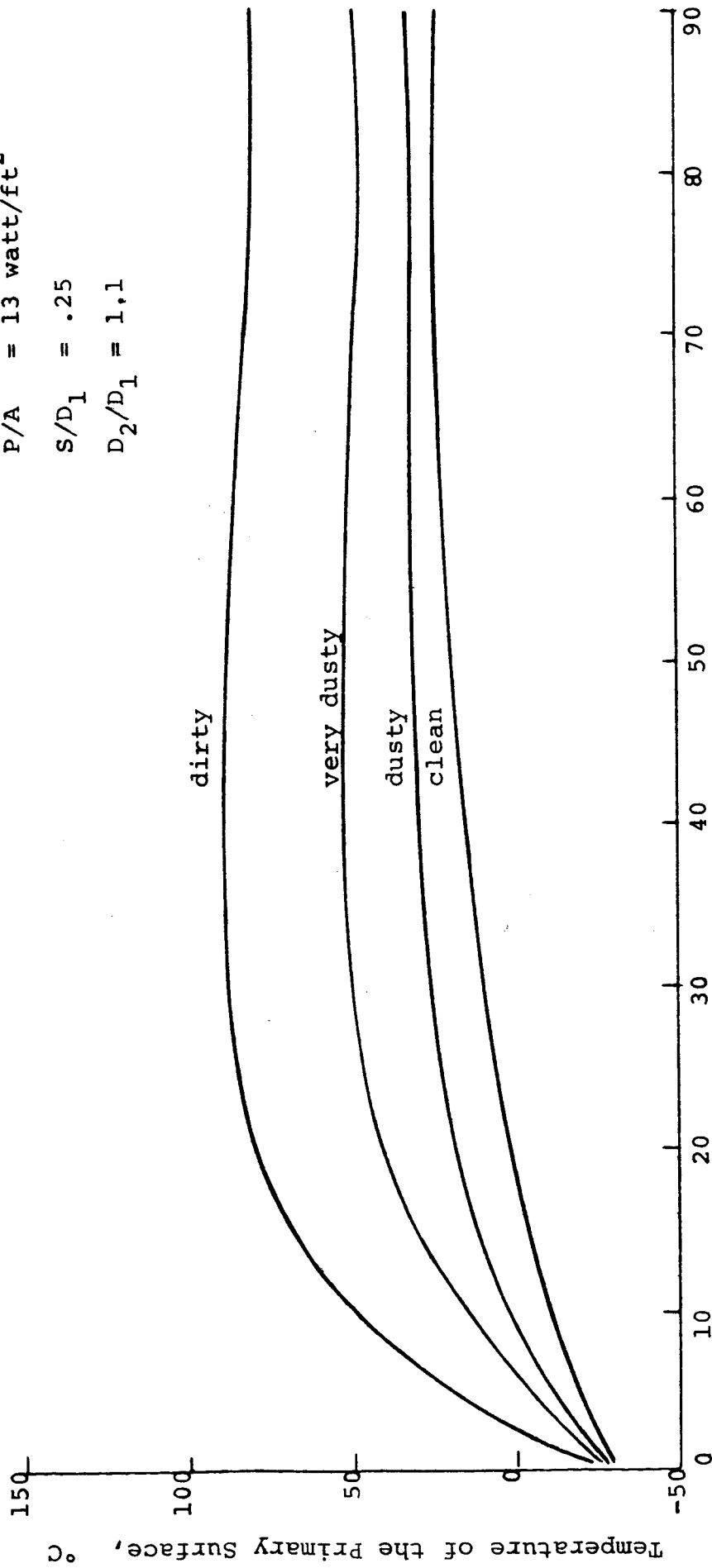


Figure 3.14

Dual Surface Configuration with
Optimum Values of S/D_1 and D_2/D_1

$P/A = 13 \text{ watt/ft}^2$
 $S/D_1 = .25$
 $D_2/D_1 = 1.1$



Solar Elevation, degrees

Figure 3.15

Thermal Performance of Optimum Dual Surface Configuration, Example No. 3

The maximum temperature for very dusty conditions is 53°C which is only 3° above the allowable maximum for the SEP receiver. The minimum temperature is -31°C which is much too low but it should be noted that this temperature rises quickly to 6°C at 25° solar elevation under clean conditions. Thus, for applications not requiring operational temperatures at low solar elevations such a design would be acceptable. Section 5.0 discusses several methods of raising minimum temperatures at low solar elevations.

3.4 Multi-Secondary Configurations

It has been shown that the dual surface design did help to heat the lower surface (primary) at low solar elevations and cool it under dirty conditions at high solar elevations. Accordingly, there is no a priori reason that a third, fourth, fifth, etc., parallel plate arrangement could not be added whereby each helped to control the temperature of the surface below it as shown in Figure 3.16.

A systematic computer iteration of key parameters for multi-secondary configuration of Figure 3.16 showed only marginal potential for improvement of primary surface thermal performance and; therefore, a discussion of equilibrium equations and optimization parameters are omitted. However, for the sake of completeness, the results are included as example No. 4.

The configuration of example No. 4 is shown in Figure 3.17. It is identical to example No. 1 except that an additional flat

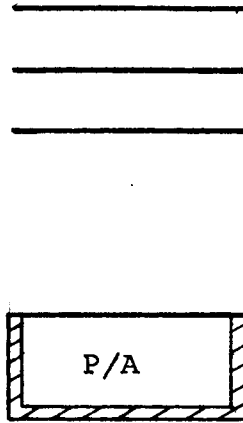


Figure 3.16

Multi-Secondary Configuration

$$P/A = 13 \text{ watt/ft}^2$$

$$D_3 = D_2 = D_1$$

$$S/D_1 = .4$$

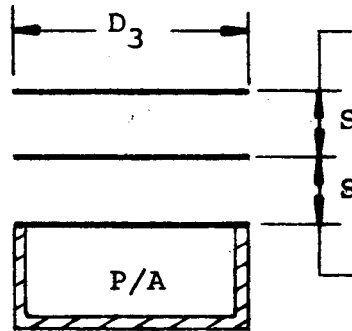


Figure 3.17

Multi-Secondary Configuration, Example No. 4

plate has been added above the original secondary. The thermal performance of example No. 4 is shown in Figure 3.18. Relative to example No. 1, the multi-secondary configuration has a slightly higher (approximately 3°C) minimum temperature, a slightly higher maximum temperature, and a much lower (approximately 30°C) temperature of the primary surface at high sun elevations. The effect of the extra surface is to accentuate the "hump" in the thermal performance curve of example No. 1

Example No. 4 is not a truly optimum design for a multi-secondary configuration. Numerical results did indicate that an optimum design is capable of slightly improving thermal performance at all solar elevations although the reduction in maximum temperature of the primary surface is only a few degrees centigrade.

$$P/A = 13 \text{ watt/ft}^2$$

$$S/D_1 = .4$$

$$D_3 = D_2 = D_1$$

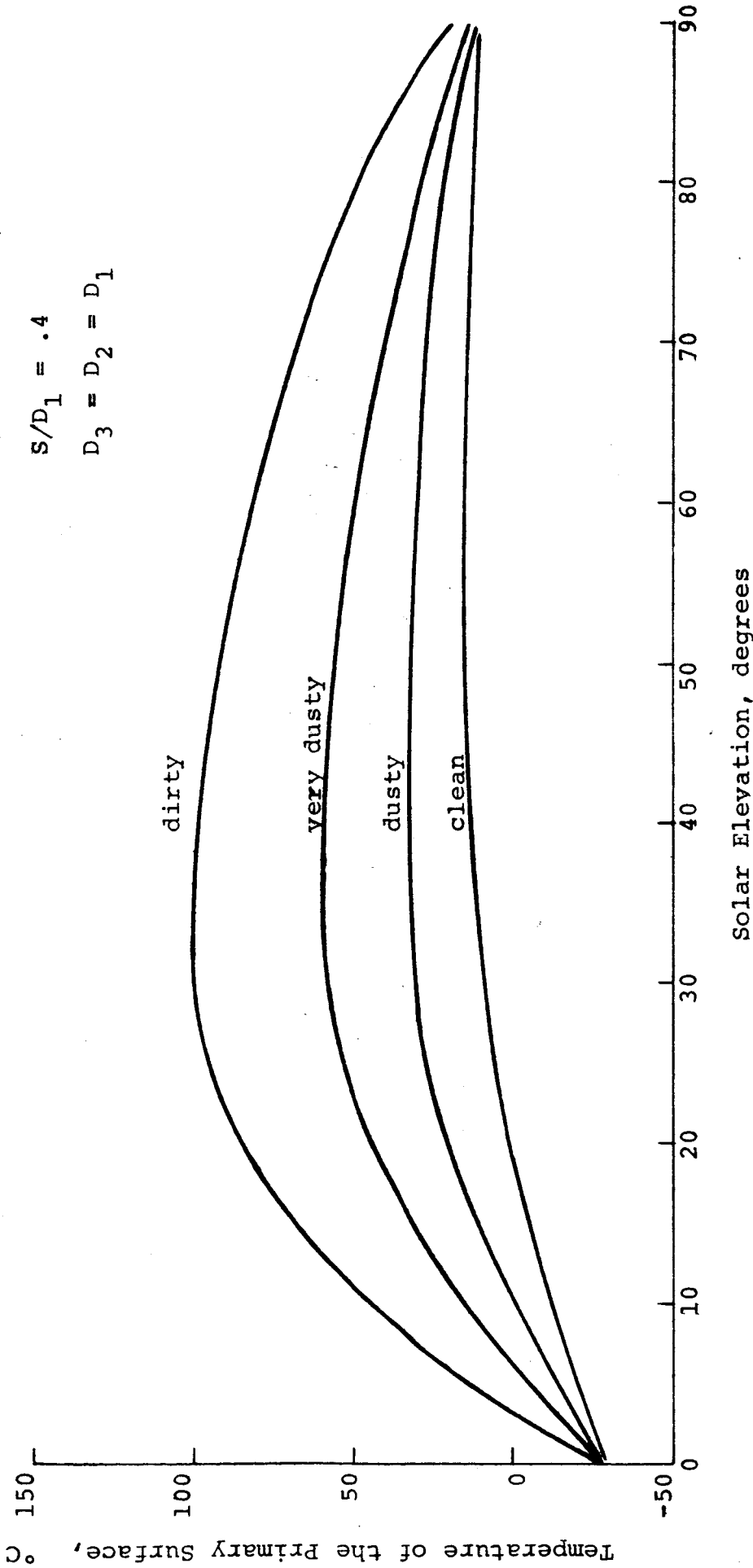


Figure 3.18

Thermal Performance of Multi-Secondary Dual Surface Configuration, Example No. 4

4.0 CONICAL SECONDARY SURFACES

4.1 Introduction

Basically, the performance of the planar dual surface configuration can be improved by raising the minimum temperature of the primary surface at low solar elevations and lowering the maximum temperature of the primary surface which, in general, occurs at about 30 to 45 degrees solar elevation. In this section, we discuss a conical secondary surfaces to achieve this objective.

Consider the dual surface configuration shown in Figure 4.1. At low solar elevations, as illustrated in Figure 4.2, one side of the cone absorbs solar energy whereas a flat plate secondary does not. On the other hand at high solar elevations the effective absorbing area of the cone is the same as that for a flat plate. The net result is a higher minimum temperature for the primary surface at low solar elevations. However, the radiative area of the conical surface is much greater than the surface area of a flat plate and, in addition, the conical surface absorbs lunar IR. It will be shown both analytically and quantitatively that at high solar elevations the increase in radiative area is more significant than the increase in absorption of lunar IR and this results in a lower maximum temperature of the primary surface.

4.2 Analytic Development, High Solar Elevations

The following brief analytic development serves to demonstrate the physical mechanism by which conical secondaries improves upon

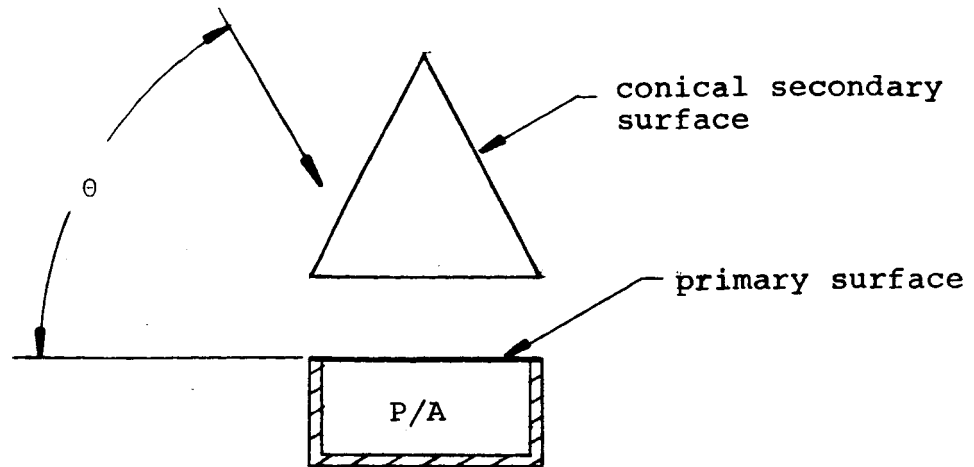


Figure 4.1

Dual Surface Model with Conical Secondary Surface

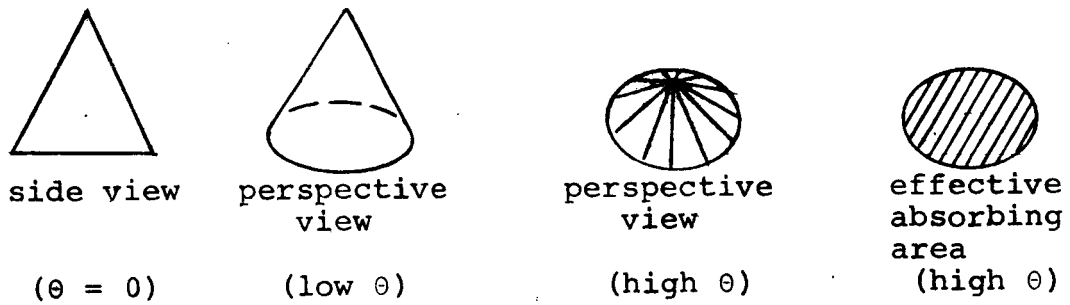


Figure 4.2

Effective Absorbing Area of a Cone at High Solar Elevations

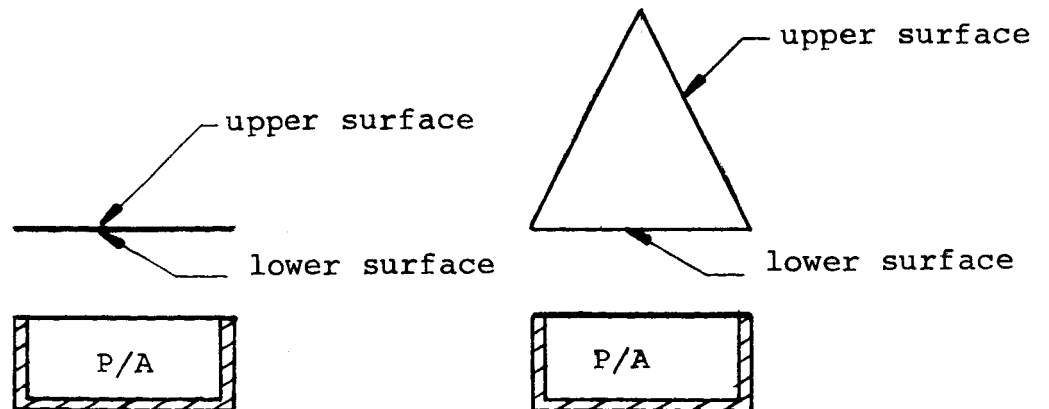


Figure 4.3

Upper and Lower Secondary Surface

the performance of the flat plate secondary and also provides a check on the consistency of the computer results which are described in Section 4.4.

Conical and flat plate secondaries may be compared at a given solar elevation by considering only the energy transfers taking place on the upper secondary surface. The distinction between "upper" and "lower" secondary surfaces in this context is defined in Figure 4.3.

Figure 4.4 shows a conical secondary insulated on the bottom so that energy transfers of the upper surface alone maybe considered. For $\beta = 180^\circ$, this secondary becomes a flat plate and for $\beta = 90^\circ$, it becomes an infinite cylinder. The thermal equilibrium equation for this conical surface allows direct comparison of flat plates, cones, and cylinders as means of controlling secondary surface temperatures at a given solar elevation.

The thermal equilibrium equation for Figure 4.4 is

$$\left[\begin{array}{c} \text{energy} \\ \text{radiated} \end{array} \right] = \left[\begin{array}{c} \text{solar energy} \\ \text{absorbed} \end{array} \right] + \left[\begin{array}{c} \text{lunar IR} \\ \text{absorbed} \end{array} \right]$$

$$\sigma \epsilon_2 T_2^4 A_{2T} = G \alpha_2 A_{\text{eff}} + \sigma \epsilon_L T_L^4 A_{2T} F_{2TL} \epsilon_2 \quad (4.1)$$

where F_{2TL} is the geometric view factor representing the fraction of energy emitted by the upper conical surface that is incident on the lunar surface. (Note that equation 4.1 uses the identity $A_L F_{L2T} = A_{2T} F_{2TL}$ in Reference 4).

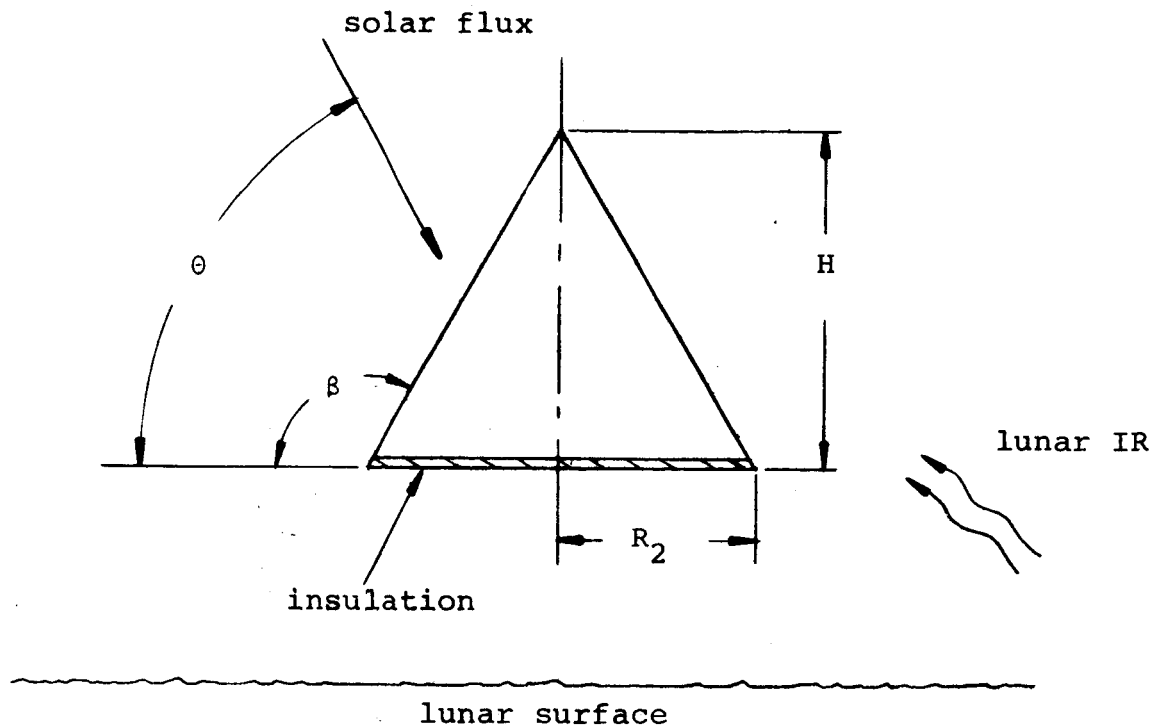


Figure 4.4

Conical Secondary Surface Neglecting Interactions at the Bottom Surface

$P/A = 13 \text{ watt/ft}^2$
 $\beta = 120^\circ$
 $S/D_1 = .25$
 $D_2/D_1 = 1.0$

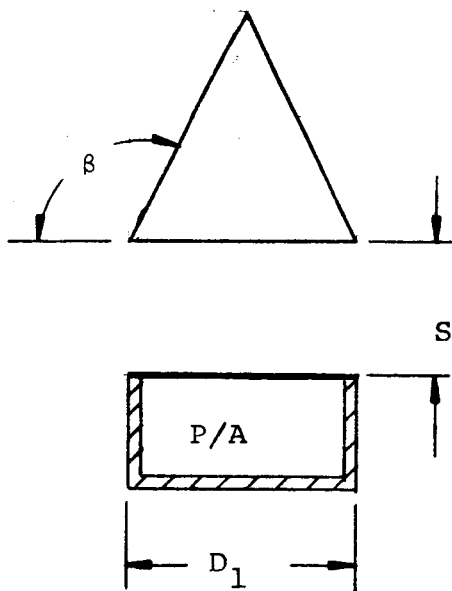


Figure 4.5

Optimum Dual Surface Configuration with Conical Secondary, Example No. 5

$$T_2 = T_L \left[\frac{R_2}{\sqrt{R_2^2 + H^2}} (\alpha_2^{-1/2} \epsilon_2) + 1/2 \epsilon_2 \right]^{1/4} \quad (4.2)$$

where $\alpha_L = 1.0$

$$\epsilon_2 = \epsilon_L = .85$$

$$\text{and } T_L = \sqrt{\frac{G \alpha_L \sin(\theta)}{\sigma \epsilon_L}}$$

From equation 4.2, as the value of H becomes very large, the quantity $\frac{R_2}{\sqrt{R_2^2 + H^2}} (\alpha_2^{-1/2} \epsilon_2)$ approaches zero. This quantity may

approach zero from the positive or negative side depending on the values of α_2 and ϵ_2 . For highly degraded surfaces, $\alpha_2 > 1/2 \epsilon_2$ and the expression is always positive. Under these circumstances, T_2 is a minimum for large values of H. Conversely, for clean surfaces ($\alpha_2 < 1/2 \epsilon_2$) T_2 is a minimum for $H = 0$.

The physical mechanism that allows T_2 to be minimized is the radiative surface area which contributes the term $\sqrt{R_2^2 + H^2}$ to the denominator of equation 4.2. For $\pi - \beta \leq \theta \leq \beta$, the conical secondary absorbs the same amount of solar energy as a flat plate but has a larger radiative surface area. The conical secondary also absorbs more lunar IR but the increased absorption is not as significant as the increase in radiative power.

Equation 4.2 cannot be used to compare the overall thermal performance of conical secondaries since the restriction $\theta > \pi - \beta$

$$F_{2TL} = 1/2 (1 + \cos \beta) = 1/2 \left(1 - \frac{R_2}{\sqrt{R_2^2 + H^2}}\right) \quad (4.1A)$$

A_{2T} = (total conical surface area)

$$= \pi R_2 \sqrt{R_2^2 + H^2} \quad (4.2B)$$

A_{eff} = (effective absorbing area of a cone)

$$= \pi R_2^2 \sin(\theta) \text{ for } \pi - \beta \leq \theta \leq \beta \text{ and } \beta \geq \frac{\pi}{2} \quad (4.1C)$$

Substitution of equations (4.1A), (4.1B), and (4.1C) in (4.1) gives

$$\begin{aligned} \sigma \epsilon_2 T_2^4 \pi R_2 \sqrt{R_2^2 + H^2} &= G \alpha_2 \pi R_2^2 \sin(\theta) \\ &+ \sigma \epsilon_L T_L^4 \pi R_2 \sqrt{R_2^2 + H^2} \quad 1/2 \left(1 - \frac{R_2}{\sqrt{R_2^2 + H^2}}\right) \epsilon_2 \end{aligned} \quad (4.1.4)$$

In (4.1.4), the term $\sigma \epsilon_L T_L^4$ represents lunar emission per unit area which under thermal equilibrium is the same as solar absorption per unit area by the lunar surface.

$$\text{Mathematically, } \sigma \epsilon_L T_L^4 = G \alpha_L \sin \theta \quad (4.1D)$$

where α_L = lunar absorptivity

Substituting (4.1D) in (4.1E) and solving for T_2 , we get

$$T_2^4 = \frac{G \pi R_2 \sin(\theta)}{\sigma \epsilon_2 \pi R_2} \left[\frac{R_2^{\alpha_2 + \alpha_L} \sqrt{R_2^2 + H^2} \quad 1/2 \quad \epsilon_2^{-\alpha_L} \frac{1}{2} R_2 \epsilon_2}{\sqrt{R_2^2 + H^2}} \right]$$

omits low solar elevations from consideration. For cones with large values of H , the omitted values of solar elevation become quite important since the omitted elevations include those at which the maximum temperatures of the primary surface occur. A rigorous analysis, valid at all solar elevations, requires the use of a general treatment for the effective absorbing area of a conical surface (A_{eff}) which is given in Appendix B. The comparison of conical secondaries using a general formulation for A_{eff} is much more complex than the preceding analysis which has been restricted to $\pi - \beta \leq \theta \leq \beta$. For this reason the general analysis will be carried out numerically on a computer. The necessary equilibrium equations for the general comparison are given in Section 4.3 and the conclusions based on the computer results are presented in Section 4.4.

4.3 Generalized Thermal Equilibrium Equations

The thermal equilibrium equations for the configuration of Figure 4.1 may be written as follows.

Equilibrium of the primary surface:

$$\left[\begin{array}{l} \text{energy} \\ \text{radiated} \end{array} \right] = \left[\begin{array}{l} \text{solar energy} \\ \text{absorbed} \end{array} \right] + \left[\begin{array}{l} \text{internal} \\ \text{dissipation} \end{array} \right] + \left[\begin{array}{l} \text{secondary IR} \\ \text{absorbed} \end{array} \right] \quad (4.3)$$

Equilibrium of the secondary surface:

$$\left[\begin{array}{l} \text{energy radiated} \\ \text{(all surfaces)} \end{array} \right] = \left[\begin{array}{l} \text{direct solar} \\ \text{energy absorbed} \end{array} \right] + \left[\begin{array}{l} \text{solar energy reflected} \\ \text{from primary surface} \end{array} \right] \\ + \left[\begin{array}{l} \text{lunar albedo} \\ \text{absorbed} \end{array} \right] + \left[\begin{array}{l} \text{lunar IR} \\ \text{absorbed} \end{array} \right] + \left[\begin{array}{l} \text{IR from primary} \\ \text{surface absorbed} \end{array} \right] \quad (4.4)$$

The general form of the equilibrium equations for conical secondaries remains the same as for planar secondaries in Section 3.0. Only three terms of equation 4.4 require formulation different from the equilibrium equations for planar dual surface configurations. They are:

$$\begin{aligned} \text{energy radiated} &= \sigma \epsilon_2 (A_{2B} + A_{2T}) T_2^4 \\ \text{all surfaces} & \\ \text{direct solar energy} &= G_{\alpha} s_2 A_{\text{eff}} \\ \text{absorbed} & \end{aligned} \quad (4.5)$$

$$\text{lunar IR} = \sigma \epsilon_L (A_{2B} F_{2BL} + A_{2T} F_{2TL}) T_L^4 \epsilon_2 \\ \text{absorbed}$$

where A_{2B} = area of the bottom of the secondary surface

A_{2T} = area of the upper secondary surface

A_{eff} = effective absorbing area of the secondary

F_{2BL} = geometric view factor of the bottom of the secondary to the lunar surface (Reference 4).

The normalization of these equations follows in the same manner as for planar dual surface configurations by defining

$$\begin{aligned} A_{2B} &= k_{12B} A_1 \\ A_{2T} &= k_{12T} A_1 \\ A_{\text{eff}} &= k_{12T} A_1 \end{aligned} \quad (4.6)$$

The normalized equilibrium equations for dual surface configurations with conical secondaries follow from equations 3.10, 3.11, 4.5 and 4.6.

Equilibrium of the primary surface:

$$\sigma \epsilon_1 T_1^4 = G \alpha_{s1} k_{1x} \sin(\theta) + \frac{P}{A} + \sigma \epsilon_2 k_{12B} F_{2B1} T_2^4 \epsilon_1 \quad (4.7)$$

Equilibrium of the secondary surface:

$$\begin{aligned} \sigma \epsilon_2 (k_{12B} + k_{12T}) T_2^4 = & G \alpha_{s2} k_{12\text{eff}} + G(1 - \alpha_{s1}) k_{1x} \sin(\theta) \\ & + \sigma \epsilon_L (k_{12B} F_{2BL} + k_{12T} F_{2TL}) T_L^4 \epsilon_2 + \sigma \epsilon_1 T_1^4 F_{12B} \epsilon_2 \end{aligned} \quad (4.8)$$

where the albedo term is included in the lunar IR term by setting $\alpha_L = 1.0$.

Equations 4.7 and 4.8 have been used to calculate the thermal performance of conical dual surface configurations in the computer analysis described in the following section.

4.4 Computer Analysis

This section presents the results of a systematic computer study based on equations 4.7 and 4.8 with the objective of identifying the shape of the conical secondary that yields the best overall thermal performance. General observations concerning conical secondaries are made and a specific example is discussed but detailed presentation of numerical results is not included.

4.4.1 Cylindrical Secondaries - A comparison based on numerical results of cylindrical configuration relative to flat plate and conical shapes is given in Table 4.1.

Comparative Thermal Performance of Cylindrical
Secondaries to Flat Plate and Conical Secondaries

Solar elevation	Temperature of the primary surface using cylindrical secondary (relative to flat plate or conical secondaries)	
	clean	dirty
0°	no change	raises
Elevation at which maximum temperatures occur	raises	raises
90°	raises	lowers

Table 4.1

Three significant observations may be made concerning cylindrical secondaries: 1.) The results of Table 4.1 are consistent with previous conclusions drawn from equation 4.2; 2.) Since the maximum temperature is increased slightly and the minimum temperature is relatively unaffected under clean conditions, the cylindrical secondary is an inferior choice; 3.) The increase in temperature at $\theta = 45^\circ$ could not have been predicted from equation 4.2 since the requirement $\theta \geq \pi - \beta$ is not satisfied.

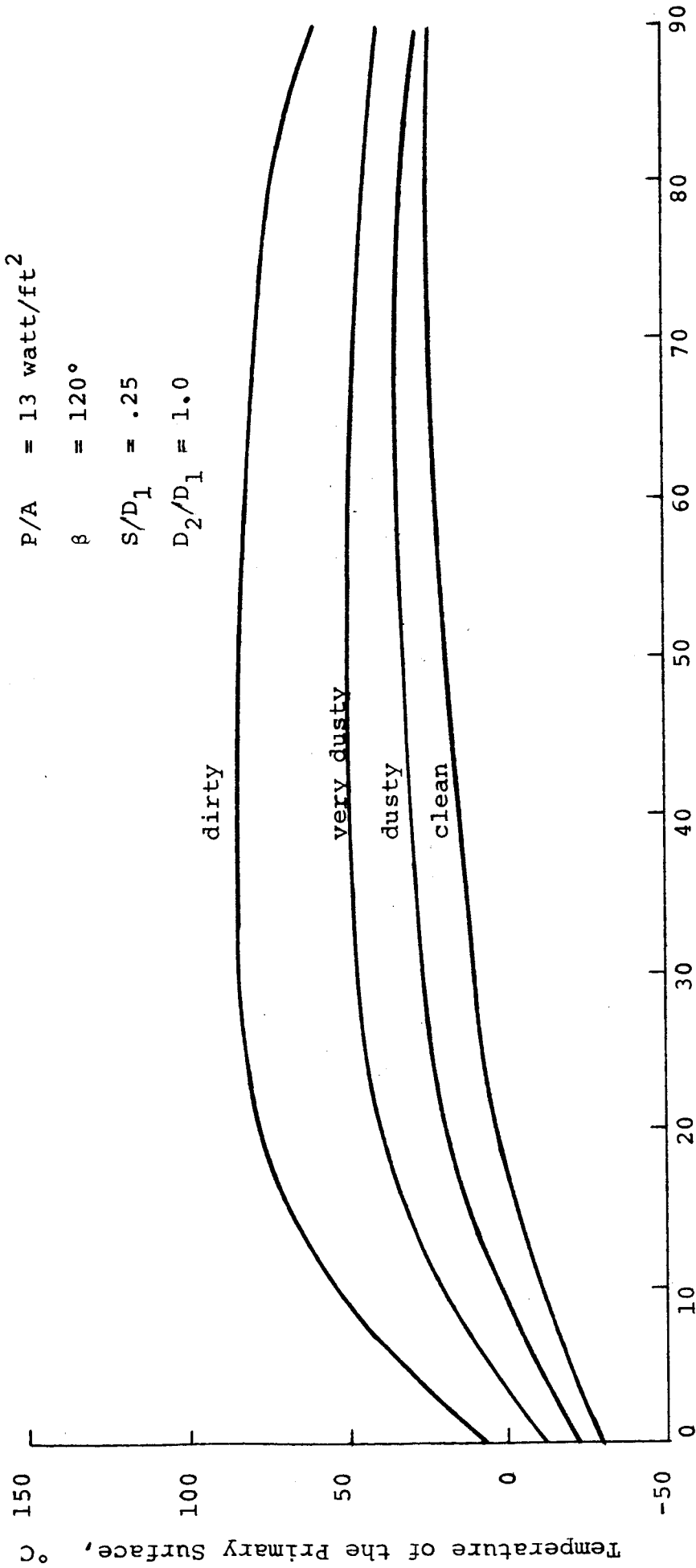
4.4.2 Conical Secondaries - Conical secondaries have the same qualitative effects in thermal performance as cylindrical secondaries (see Table 4.1) except that the maximum temperature

under degraded conditions which is lower for certain conical secondaries.

The maximum temperature of the primary surface under degraded conditions is slightly less than for flat plate and cylindrical secondaries but only for a small range of the angle β (approximately 110° to 130°). This range represents the best tradeoff of solar and lunar IR absorption at the solar elevation for which maximum temperatures of the primary surface occur. The optimum value of β changes slightly with surface conditions but not enough to warrant consideration.

The computer results for conical secondaries are again consistent with equation 4.2. First, for $\beta = 180^\circ$, the results agree with previous results for flat plate designs. Second, increasing the value of H always decreases temperatures of the primary surface under degraded conditions for $\pi - \beta \leq \theta \leq \beta$ and $\frac{\pi}{2} \leq \beta \leq \pi$.

4.4.3 Optimum Conical Secondary - Example No. 5 (Figure 4.5) represents a conical dual surface configuration with the best values of the separation parameter (S/D_1) and the conical angle (β) as determined from numerical computer results for several iterations of S/D_1 and β using equations 4.7 and 4.8. The parameter D_2/D_1 is set equal to one and not iterated since it has been shown (Section 3.0) to have little effect on dual surface optimization. The parameter P/A is set at the value of 13 watts/ft² for purposes of comparison with previous examples. Figure 4.6 shows the thermal performance of the example No. 5.



Solar Elevation, degrees

Figure 4.6

Thermal Performance of Dual Surface Configuration with Optimum Conical Secondary, Example No. 5

The thermal performance of this configuration is acceptable except at low solar elevations. For clean, dusty, and very dusty conditions the maximum temperature is less than 50°C. At solar elevations less than 30°, the minimum temperature of the primary surface is below 5°C and must be raised in order to satisfy thermal requirements of the SEP receiver.

5.0 EXTENSIONS

Table 5.1 is intended as a summary of the relative performance of the various configurations.

Also, this section briefly describes several other ideas for improving the thermal performance of simple dual surface configuration. It is intended as a guide for future work and, as such, attempts to convey concepts rather than quantitative results. It is felt that these ideas offer potential for designing lightweight thermal protection systems for electronic packages intended of mobile use in the dusty lunar environment.

5.1 Solar Powered Heater

One method of raising the minimum temperature of any configuration is to use solar cells to power an internal heater. This method would seem to have an advantage over alternatives such as a mechanical thermal switch because an electronic thermostat (switch) is probably inherently more reliable than a mechanical thermal switch. The major disadvantages of solar cells is the relative larger size and weight requirements for the solar panel due to the relatively low (10%) efficiency of energy conversion.

An example (Figure 5.1) has been studied to determine the feasibility of this system. The following items were considered:

- (a) the degradation of solar cell performance under high temperatures,
- (b) the degradation of solar cell performance under dusty conditions,
- and (c) solar panel size required for achieving the minimum allowable temperature at low solar elevations.

TABLE 5.1 - THERMAL PERFORMANCE OF EXAMPLE CONFIGURATIONS

Example	Configuration	Parameters		Minimum Temperature °C, Clean	Maximum Temperature (°C) very dusty	Maximum Temperature (°C) dirty
		P/A (wt/ft ²)	S/D ₁			
-	Simple radiative surface	13	-	-41	74	140
		6.5	-	-78	65	134
#1	Typical Dual Surface	13	.4	-35	56	100
#2	Typical Dual Surface, low P/A ratio	6.5	.4	-72	45	92
#3	Optimum Dual Surface	13	.25	-31	53	89
#4	Multi-secondary	13	.4	-33	58	101
#5	Optimum conical secondary ($\beta=120^\circ$)	13	.25	-29	50	83
#6	Optimum conical secondary with solar powered heater ($\beta=120^\circ$, $H_p = D_1$)	13	.25	8	50	83

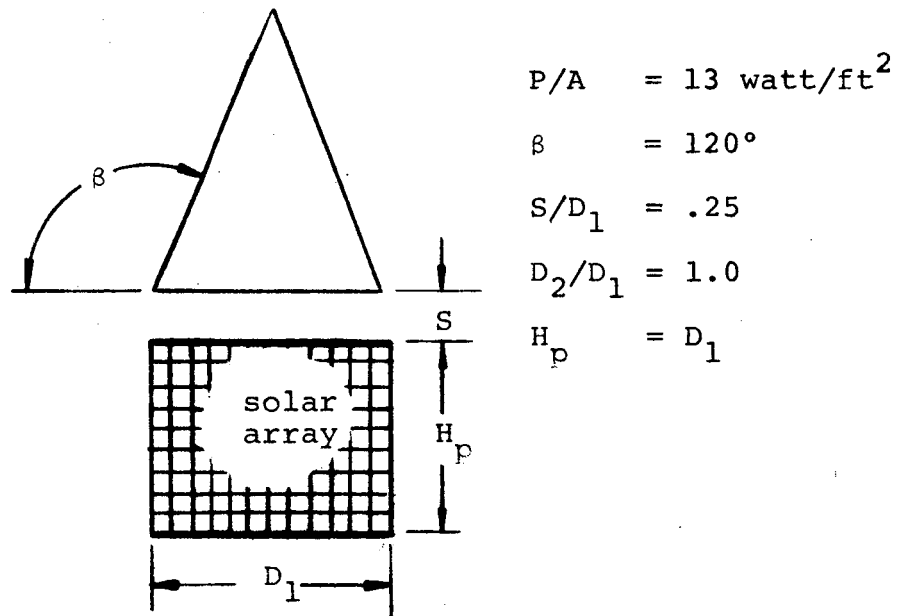


Figure 5.1

Dual Surface Design with Solar Powered Heater, Example No. 6

The following assumptions have been made for this example:

1. Change from the nominal solar cell efficiency (10%) are linear with degrading surface conditions; i.e., a linear decrease from this 10% efficiency for clean conditions to 0% efficiency for dirty conditions.
2. Degradation of solar efficiency is $-.54\%$ per degree centigrade above 27.8°C where the temperature of the solar array is determined on the basis of $\alpha_s = .85$, $\epsilon = .85$ for all dust conditions.
3. The heater is controlled by an electronic thermostat (transistor and thermistor) set at 25°C which was chosen to be consistent with the thermal requirements of the receiver.

The purpose of example No. 6, which is dimensioned as shown in Figure 5.1, is to demonstrate the performance of a typical configuration designed to meet the SEP receiver requirements. This configuration is identical to example No. 5 except for the addition of the solar powered heater. The thermal performance of example No. 6 is shown in Figure 5.2. For clean conditions, the heater results in a flat curve at 25°C . For dusty, very dusty, and dirty conditions, the minimum temperature is less than 25°C at low solar elevations because under these conditions, the efficiency of the solar array is degraded and cannot supply enough electrical energy to heat the internal electronics. An interesting point is that for dirty conditions where the solar array is completely ineffective, the conical secondary absorbs enough solar energy to maintain minimum SEP thermal requirements (5°). The solar array has no effect on temperatures above 25°C because the thermostat turns the heater off. This configuration satisfies thermal requirements for

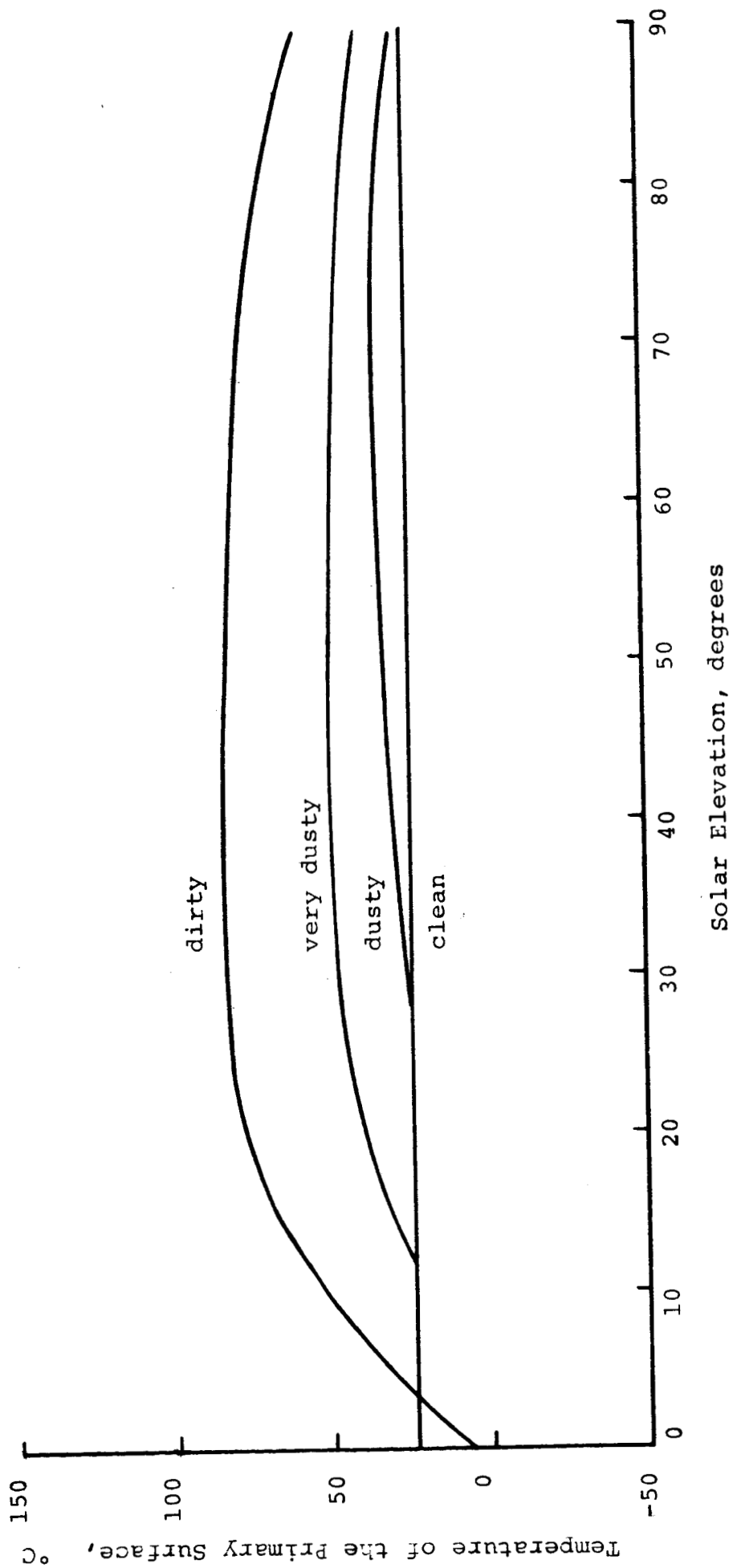


Figure 5.2
 Thermal Performance of Conical Dual Surface Configuration
 with Solar Powered Heater, Example No. 6

the SEP receiver under clean, dusty, and very dusty conditions but unfortunately, the maximum allowable temperature (50°C) is exceeded for dirty conditions.

5.2 Variable Area Systems

Variable area systems are another means of controlling the temperature of the primary surface. By reducing the area of the primary surface at low solar elevations, the value of the ratio P/A is increased and the temperature may be increased to very high levels by allowing the area to approach zero (equation 3.14).

There are several methods for varying the area of the primary surface. One is the use of a simple bimetallic activator as shown in Figure 5.3. When the configuration is cold, the spring rotates the exposed radiative area underneath an insulating surface and replaces it with a nonradiative surface. As the temperature rises, the exposed radiative area is increased. Such a system is simple, lightweight, and has been frequently used in previous space applications.

Another way of changing the radiative area of the primary surface is to manually remove or replace insulation covers on the radiative surface in order to alter the ratio P/A . This method is limited by the amount of astronaut interaction required and requires a visible temperature indicator to insure reliable temperature control.

A fundamental limitation of all variable area surfaces is that they are only useful in increasing minimum temperatures--they

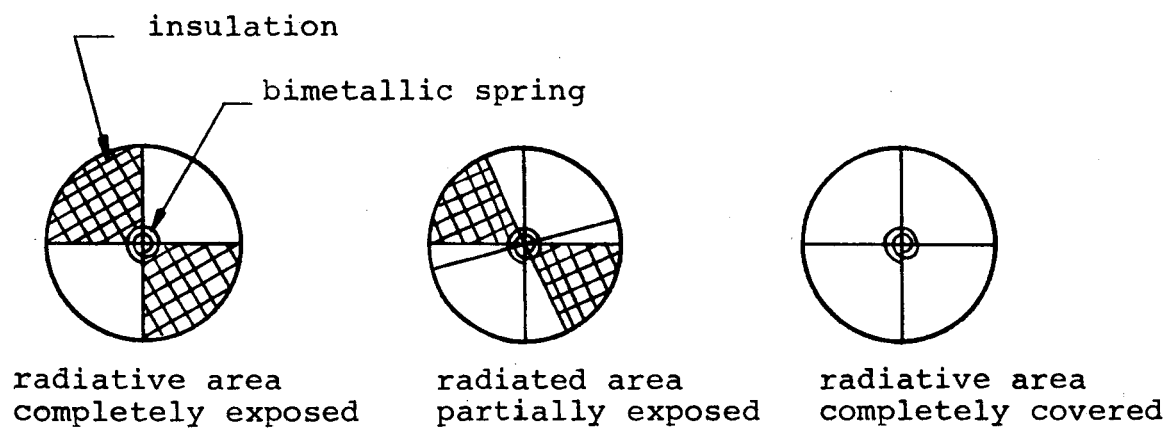


Figure 5.3

Variable Area Mechanism Using Bimetallic Spring

cannot lower the maximum temperatures below those incurred by simple radiative surfaces unless, in addition, the astronaut is required to brush the dust from the control surfaces at appropriate intervals. However, by applying both the dual surface and variable area concepts to a design, the thermal performance of the configuration can be greatly improved with respect to both the minimum and maximum temperature.

5.3 Multi-characteristic Dual Surface Configurations

The thermal performance of dual surface configurations can be improved by using materials other than second surface mirrors for selective parts of the configuration.

Consider the dual surface design of Figure 5.4. The effect of using a low emittance material for the bottom of the conical secondary is to reduce the amount of energy radiated from this surface to the primary and, in addition, to absorb less lunar IR. While both of these effects will decrease the temperature of the primary surface, the low emittance surface does reflect a large fraction of IR originating from both the lunar and primary surfaces and; therefore, the decrease in radiated energy to the primary may be offset by the increase in reflected energy.

Figure 5.5 shows a modification that does reflect nearly all IR from the primary surface "out" of the configuration but unfortunately still allows to be reflected "in".

One way of minimizing the effect of this reflected lunar IR would be to reduce the absorption of lunar IR by the secondary itself.

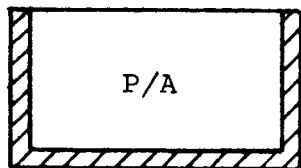
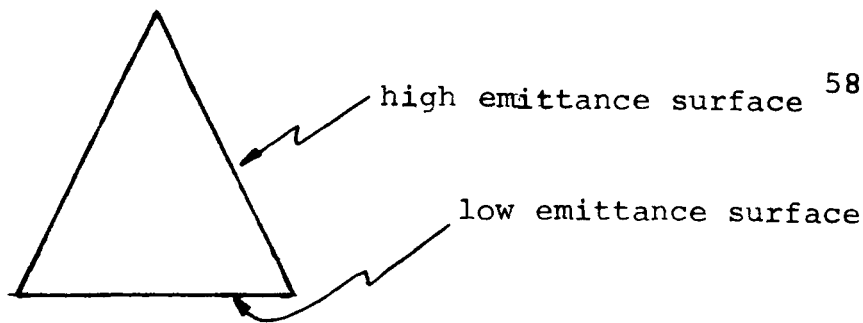


Figure 5.4

Multi-Characteristic Secondary

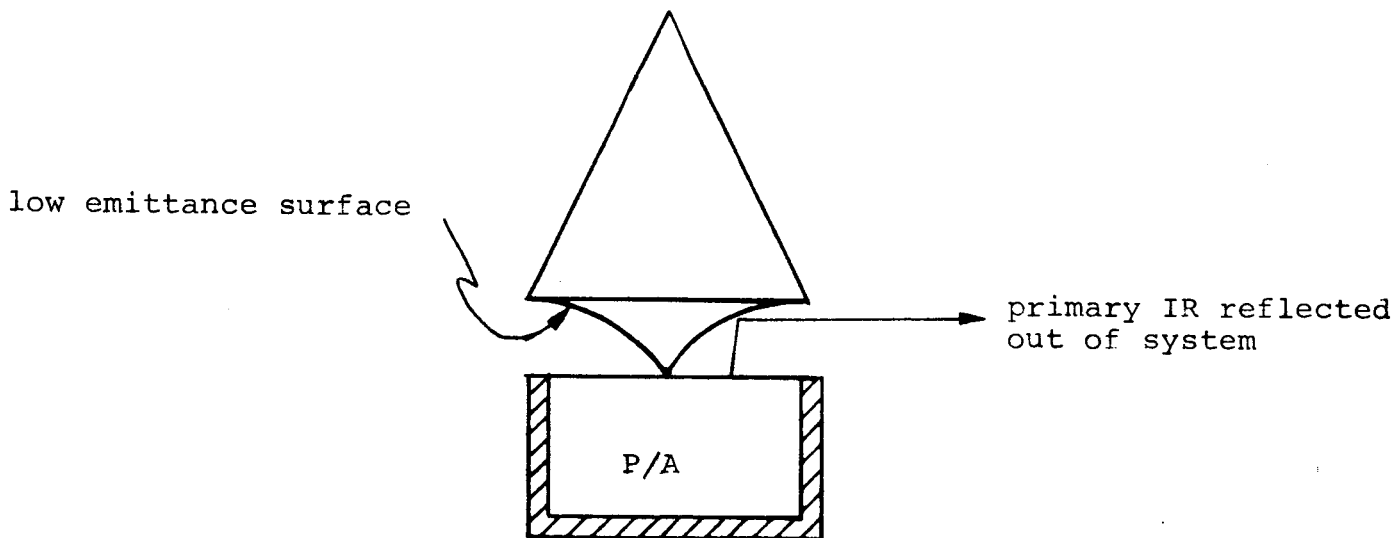


Figure 5.5

Modified Geometry of Multi-Characteristic Secondary

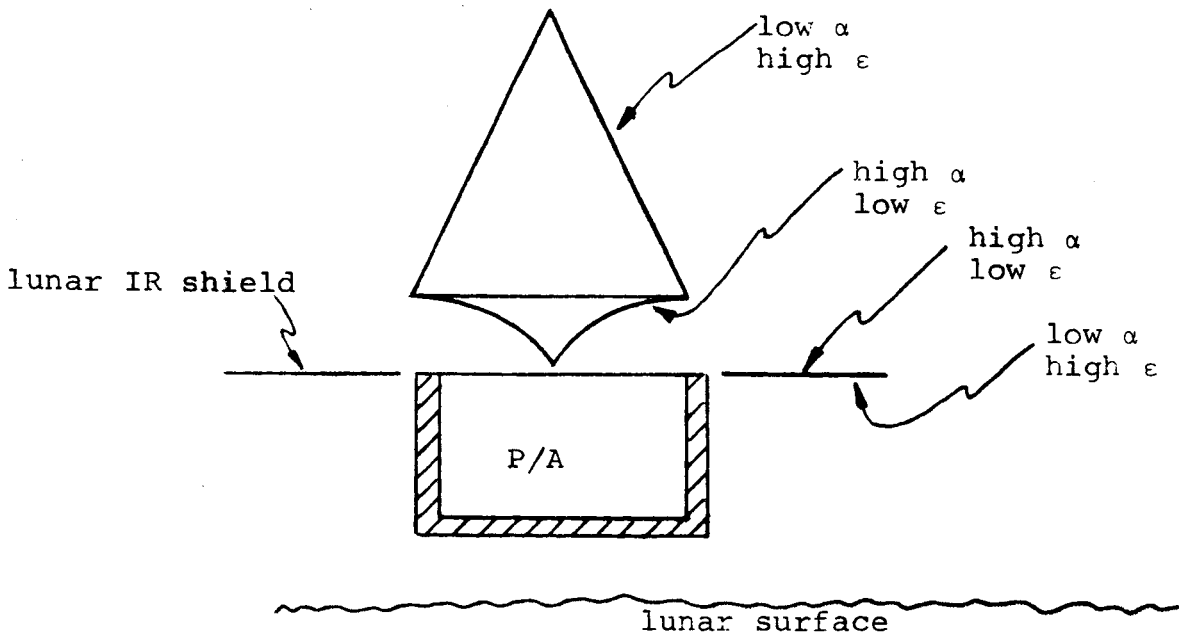


Figure 5.6

Lunar IR Shields using Multi-Characteristic Materials

It is not desirable, however, to reduce the emittance of the primary or the sides of the cone because this would cause the secondary temperature to increase. Instead, it is possible to "block" the lunar IR using multi-characteristic shields as shown in Figure 5.6. The upper surface of the shield has high absorptance to reduce the amount of solar energy reflected to the secondary and low emittance to reduce the IR energy radiated to the secondary. The bottom surface has high emittance so that a high percentage of the energy absorbed by the shield is radiated downward--away from the secondary. Again, it is important to note that these refinements are possible only if the surfaces do not become completely degraded. However, until the surfaces are completely degraded; i.e., $\alpha_s = .90$, $\epsilon = .85$, multi-characteristic materials do provide some advantage over single property materials.

5.4 Glass Surfaces

The use of transparent materials to improve thermal performance is a logical extension. The basic mechanism that enables multi-characteristic materials to improve thermal performance is the spectrally dependent nature of absorptance (α_s) and emittance (ϵ). Emittance is primarily in the infrared region while absorptance which is primarily in the visible light spectrum.

Common types of glass are also spectrally dependent. Typically, glass is highly transparent ($\tau_V \approx .90$) to visible light but nearly opaque to infrared radiation ($\tau_{IR} \approx .05$). In addition, glass, especially thermal "sandwich" glass, is a good insulator. Figure 5.7

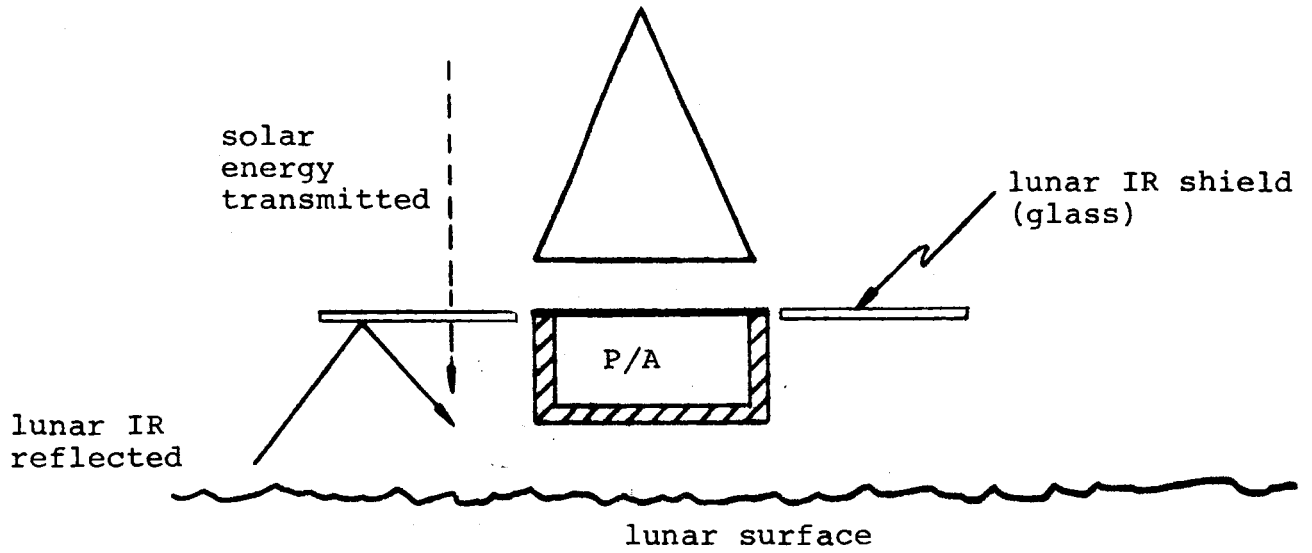


Figure 5.7

Glass used as a Lunar IR Shield

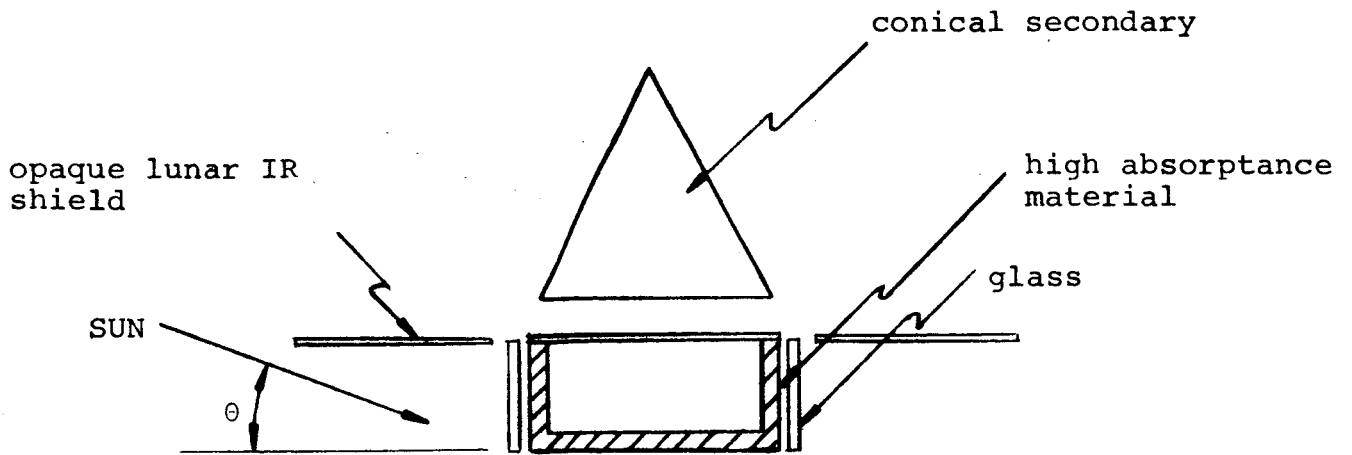


Figure 5.8

Passive Heater Design using
Glass Covered Absorbing Surface

shows the application of glass as a lunar IR shield. It is superior to a metallic IR shield in that it has the ability to limit IR incident on the secondary surface because it absorbs less energy. Under dirty conditions, of course, the performance of metallic and glass shields is the same.

Glass also offers several interesting possibilities for controlling (raising) minimum temperatures of the primary surface more efficiently than does the solar powered heaters (Section 5.1). Consider, for example, the configuration of Figure 5.8. The design is similar to example No. 6 (Figure 5.1) which was used to demonstrate the use of a solar powered heater. In this particular case, however, the glass acts both as an insulator and as an IR reflector. At low solar elevations under clean conditions, the glass transmits solar energy directly to the extended portion of the primary surface, thus, heating the configuration. As the sun rises, the extended absorbing area becomes shaded by the opaque lunar IR shield and the glass reflects lunar IR. Since the glass acts as a good insulator, the ratio P/A is not dependent on the area of the extended absorbing surface in any way.

Under dirty conditions at high solar elevations, the surface of the glass becomes highly absorptive and emissive and absorbs lunar IR but very little energy is transmitted to the underlying surface because the glass serves as a good insulator. Thus, maximum temperatures are not effected by this extension. At low solar elevations, the transmissivity of the glass becomes zero under dirty conditions and no solar energy is transmitted to the extended

primary surface. However, under these conditions, the conical secondary absorbs sufficient solar energy operating temperatures for the SEP experiment as in example No. 5.

This glass shield method for raising minimum temperatures has significant advantages over the solar powered heater. First, the efficiency of the extended absorbing surface in converting solar energy to thermal energy is approximately 80% as opposed to 10% for the solar panels. Second, the required absorbing area is much smaller (hence, less massive) than for solar panels. Third, a thermostat is not required and it becomes a completely passive design. As illustrated in Figure 5.8, the sun shield completely shades the extended absorbing surface at sun elevations just below the maximum temperature elevation.

Work has not been completed on this multi-characteristic glass shield approach and, of course, there will, in all likelihood, be some significant mechanical and material problems associated with this configuration. However, the thermal performance afforded by this method is impressive and warrants reporting and further study.

6.0 CONCLUSIONS AND RECOMMENDATIONS

1. Planar dual surface configurations improve the thermal performance of single radiative surfaces by: i) raising temperatures at low solar elevations (all surface conditions), ii) lowering temperatures at high solar elevations under dirty conditions, and iii) raising temperatures at high solar elevations under clean conditions.
2. The parameter P/A may be used to raise temperatures of the primary surface to high levels by allowing the area to approach zero. Increasing the radiative area lowers minimum temperatures more than maximum temperatures.
3. For dual surface configurations, an optimum value exists for the parameter S/D_1 that minimizes the maximum temperatures incurred and maximizes the minimum temperatures. The optimum value represents the best balance between primary surface shading and secondary IR. For $P/A = 13 \text{ watts/ft}^2$ the optimum value is $S/D_1 = .25$.
4. There is an optimum value of the parameter D_2/D_1 but its effect is insignificant compared to that of the parameters P/A and S/D_1 . For $P/A = 13 \text{ watts/ft}^2$ and $S/D_1 = .25$, the optimum value is $D_2/D_1 = 1.1$.
5. Multi-secondary configurations, using several planar surfaces, may be used to accentuate the effect of simple dual surface designs on thermal performance. This results in higher temperatures at low solar elevations and lower temperatures at high solar elevations. The effect at elevations for which maximum temperatures occur depends on the value of the parameter S/D_1 and an optimum value of S/D_1 causes the maximum temperature to decrease a few degrees centigrade.
6. A cylindrical secondary with $H \gg R$ raises the temperature of the primary surface at low solar elevations (all surface conditions) and lowers it at high solar elevations (degraded conditions only) relative to a planar secondary surface. In all cases the cylindrical secondary raises the maximum temperature of the primary surface relative to flat plate secondaries.

7. Conical secondaries have the same general effects as cylindrical secondaries and for a small range of the angle β , conical secondaries reduce somewhat the maximum temperature incurred by the primary surface. A value of $\beta \approx 120^\circ$ yields the lowest maximum temperature and represents an optimum trade-off between absorbed solar energy and absorbed lunar IR at solar elevations for which maximum temperatures occur.
8. An electric heater powered by solar cells is a feasible method of raising primary surface temperatures at low solar elevations. It is possible to satisfy SEP receiver thermal requirements for clean, dusty, and very dusty conditions using a solar powered heater in a conical dual surface configuration (Figure 5.2, Table 5.1). Under dirty conditions, the solar cells are inactive but the conical secondary absorbs enough solar energy to maintain minimum allowable temperatures. However, for dirty conditions, the maximum allowable temperature is exceeded rising to a maximum of about 83°C .
9. Further investigation of lunar dust contamination is needed. It would be desirable to know how much dust is required to cause a certain level of degradation and what circumstances would create such a dust environment. Also, it would be useful to determine the mechanism (electrical, chemical, etc.) that causes strong adherence of lunar dust to surfaces. This type of knowledge could lead to the design of nondegrading surfaces simply by preventing the accumulation of dust on surfaces.
10. The ideas discussed in Section 5.0 offer potential areas for more detailed analysis and better thermal designs. In particular, the passive heating concept using a glass covered absorbing surface and the use of multi-characteristic surfaces appear both attractive in terms of performance and practical.
11. A dual surface configuration using multi-characteristic materials with a conical secondary surface, lunar IR shields, and a glass covered absorbing surface appears to offer the best performance. Such a configuration would perform better than example No. 6 which satisfied SEP receiver requirements for clean, dusty, and very dusty surface conditions.

APPENDIX A

UNSHADED AREA OF THE PRIMARY SURFACEObjective

The objective of this appendix is to derive a general formulation for the exposed area of a circular primary surface when shaded by a circular secondary surface at varying solar elevations. Figure A.1 shows a side view of the basic dual surface model, with the notation to be used in this derivation.

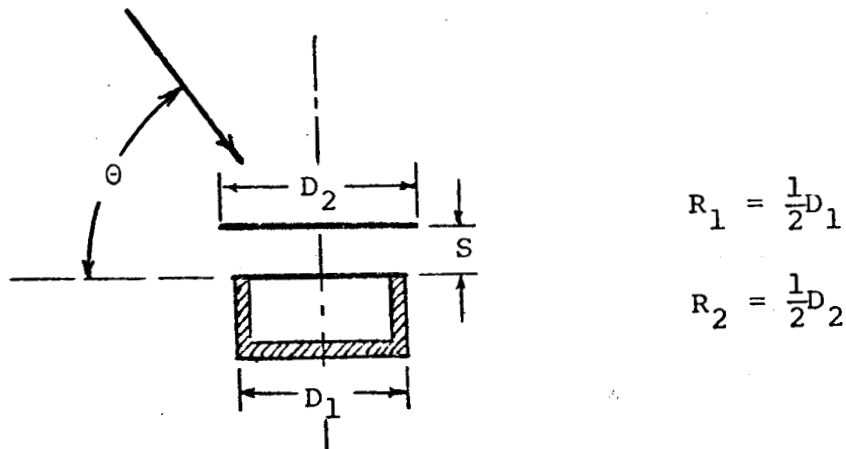


Figure A.1 - Side View of Dual Surface Model

Procedure

Figure A.2 shows the apparent displacement of secondary and primary surfaces due to solar elevation. From this figure,

$$R_1^2 = x^2 + (y + L)^2 \quad (\text{A.1})$$

$$R_2^2 = x^2 + y^2 \quad (\text{A.2})$$

and solving for the y coordinate of point P,

$$y = \frac{R_1^2 - R_2^2 - L^2}{2L} \quad (\text{A.3})$$

where R_1 = radius of the primary surface

R_2 = radius of the secondary surface

θ_1 = angle defining segment one

θ_2 = angle defining segment two

L = apparent displacement of the center of the two surfaces

$$L = S \cot(\theta)$$

A_x = the exposed area of the primary surface

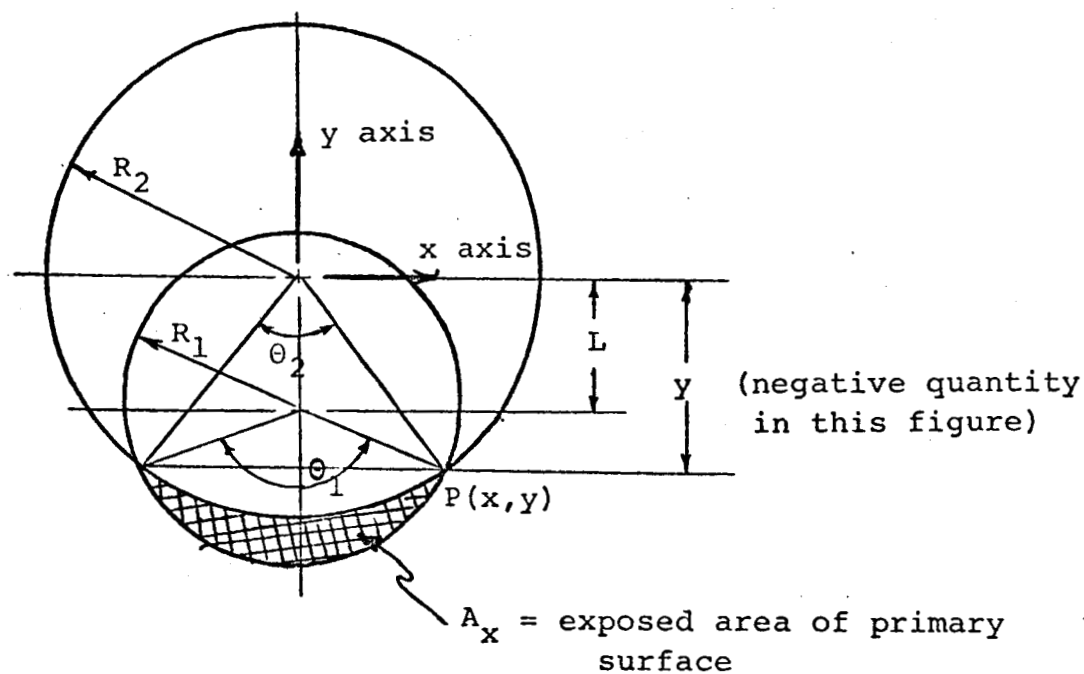


Figure A.2 - Apparent Displacement of Secondary and Primary Surfaces

Figure A.3 shows the breakdown of A_x into two segments for purposes of calculation.

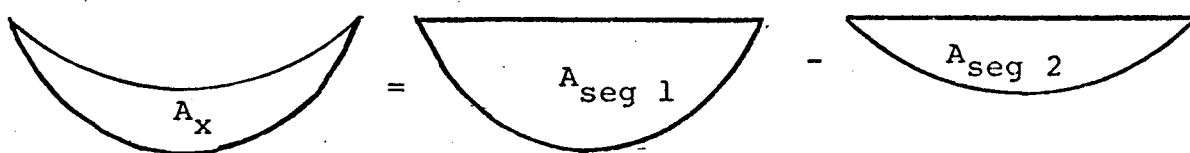


Figure A.3 - Breakdown of A_x into Segments

Calculation of $A_{\text{seg 1}}$, $A_{\text{seg 2}}$, A_x

From Figure A.3

$$A_x = A_{\text{seg 1}} - A_{\text{seg 2}} \quad (\text{A.4})$$

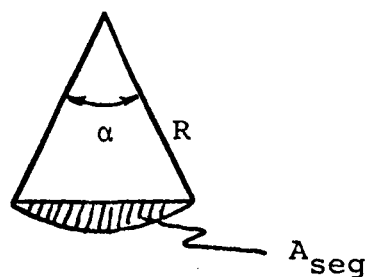


Figure A.4 - Area of a Segment

From Figure A.4, the area of a segment (A_{seg}) is given by

$$A_{\text{seg}} = \frac{\alpha}{2\pi} \pi R^2 - 1/2 R^2 \sin(\alpha) \quad (\text{A.5})$$

Segments $A_{\text{seg } 1}$ and $A_{\text{seg } 2}$ can be calculated from equation (A.5) as shown below.

$$A_{\text{seg } 2} = \frac{\pi R_2^2 \theta_2}{2\pi} + xy$$

$$A_{\text{seg } 2} = \frac{R_2^2 \theta_2}{2} + xy \quad (\text{A.6})$$

$$\text{where } \theta_2 = 2 \sin^{-1} \left(\frac{x}{R_2} \right)$$

$$x = \sqrt{R_2^2 - y^2}$$

$$y = \frac{R_1^2 - R_2^2 - L^2}{2L}$$

$$\text{Similarly, } A_{\text{seg } 1} = \frac{\pi R_1^2 \theta_1}{2\pi} + x(L + y)$$

$$A_{\text{seg } 1} = \frac{\theta_1 R_1^2}{2} + x(L + y) \quad (\text{A.7})$$

$$\text{where } \theta_1 = 2 \sin^{-1} \left(\frac{x}{R_1} \right)$$

From Equations A.4, A.6 and A.7,

$$A_x = R_1^2 \sin^{-1} \left[\frac{R_2^2 - \frac{R_1^2 - R_2^2 - S^2 \cot^2(\theta)}{2S \cot(\theta)}}{R_1} \right]$$

$$+ L \sqrt{R_2^2 - \frac{R_1^2 - R_2^2 - S^2 \cot^2(\theta)}{2L}}$$

$$- R_2^2 \sin^{-1} \left[\frac{R_2^2 - \frac{R_1^2 - R_2^2 - S^2 \cot^2(\theta)}{2S \cot(\theta)}}{R_1} \right]$$

APPENDIX B

EFFECTIVE ABSORBING AREA OF CONICAL SURFACESObjective

The objective of this appendix is to obtain a general formulation for the effective absorbing area of various conical surfaces when exposed to the solar flux at solar elevations from 0° to 90° . Several special cases of conical surfaces are shown in Figure B.1. Derivations of area for the inverted truncated cone will be shown because this surface allows the most convenient coordinate system for analysis. Results for the non-inverted cases are similar, and will be stated but not derived. Note that the non-truncated cone may be considered a special case of the truncated cone, with the radius of the truncated end equal to zero, and the cylinder a special case with equal end radii.

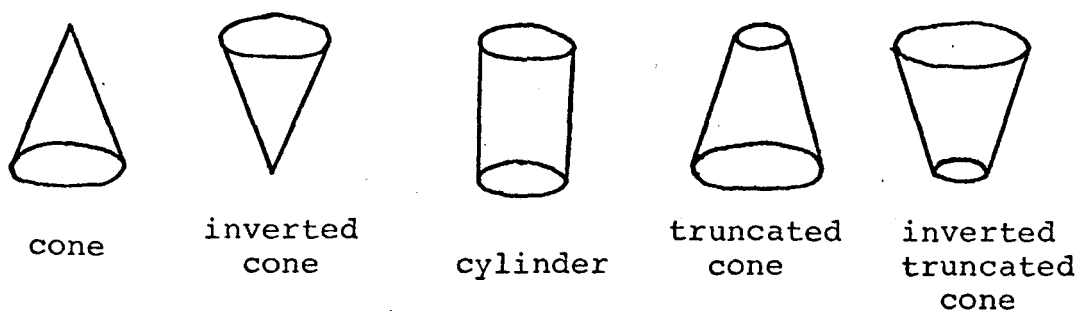


Figure B.1 - Conical Surface Considered in Appendix B

Effective absorbing area (A_{eff}) is the projected area of a conical surface exposed to direct solar flux. The area is projected in a plane normal to the solar flux. Figure B.2 shows a perspective view of the exposed area of an inverted truncated cone.

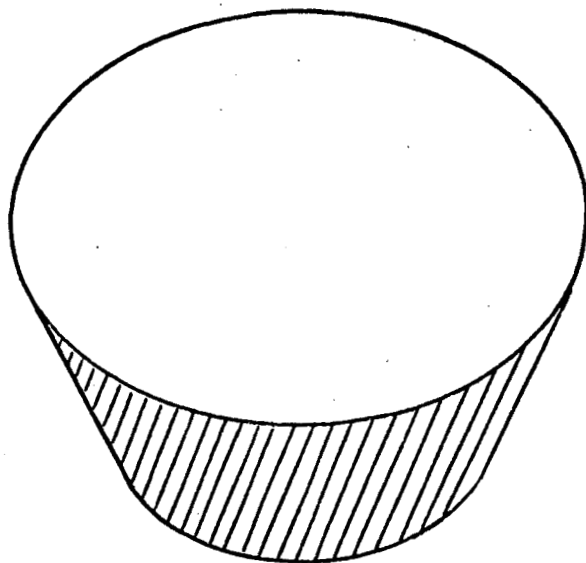
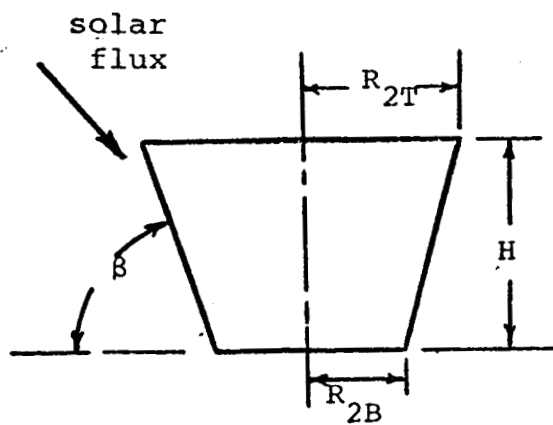


Figure B.2 - Perspective View of Absorbing Area of an Inverted Truncated Cone

Figure B.3 shows a side view of an inverted truncated cone with the notation to be used in the analysis.



- R_{2T} = radius of top of conical secondary
- R_{2B} = radius of bottom of conical secondary
- H = height of conical secondary
- β = angle of conical side with respect to horizontal

Figure B.3 - Side View of Inverted Truncated Cone

Figure B.4 shows the area projected into a plane normal to the solar flux, and set up in a coordinate system for analysis.

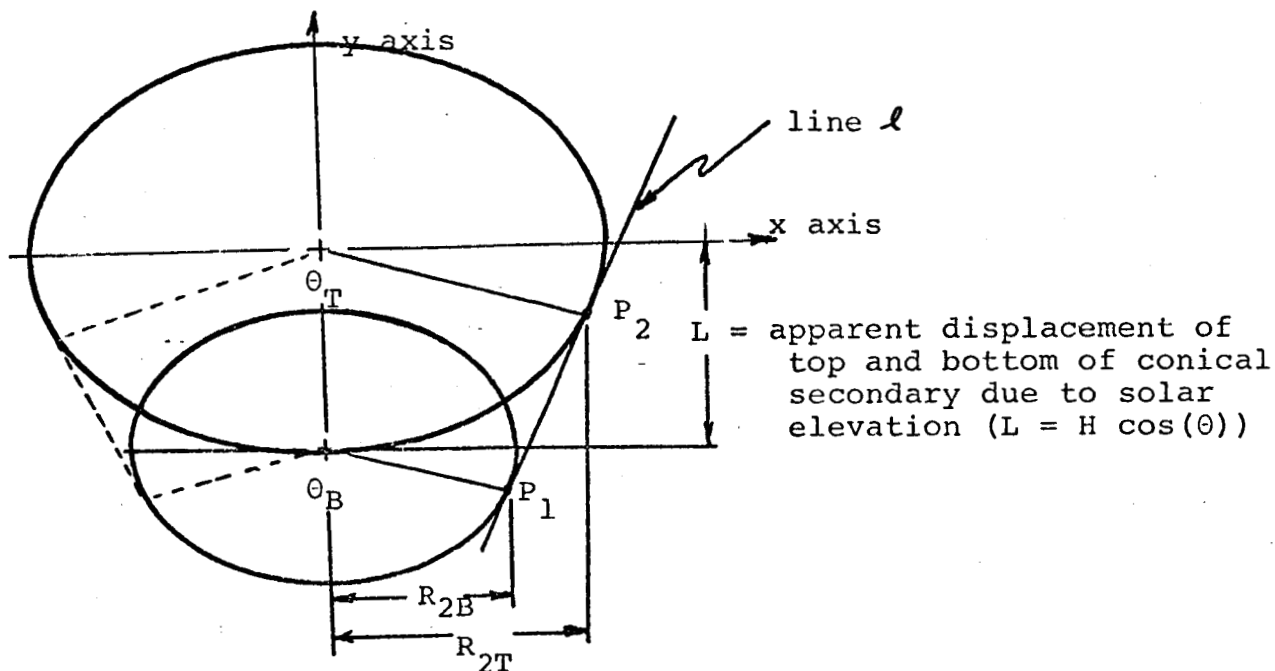


Figure B.4 - Effective Area Coordinate System

The calculation of A_{eff} may be simplified by breaking it into three segments, such that $A_{\text{eff}} = A_{\text{trap}} - A_{\text{seg t}} + A_{\text{seg b}}$ as shown in Figure B.5.

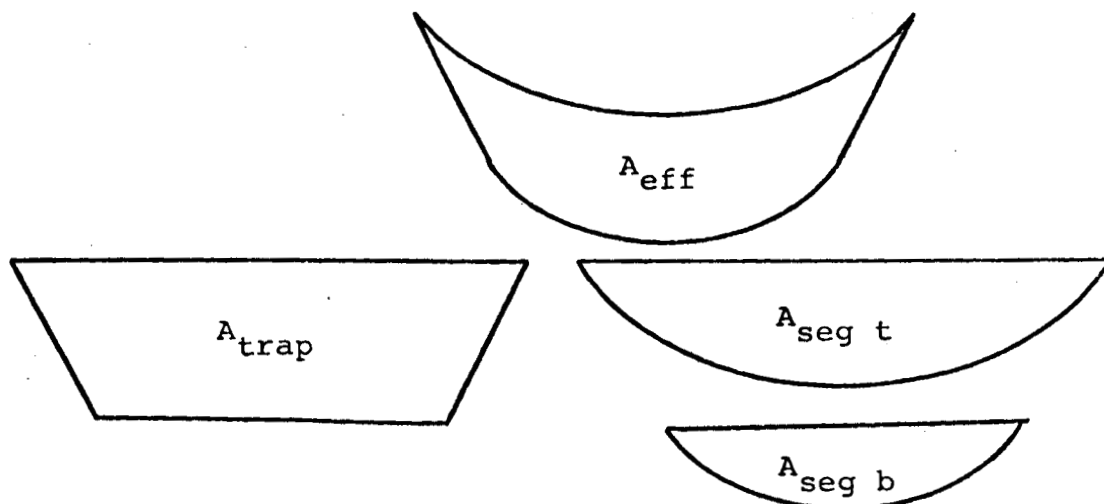


Figure B.5 - Breakdown of A_{eff} into Simpler Area

Figure B.4 shows the area projected into a plane normal to the solar flux, and set up in a coordinate system for analysis.

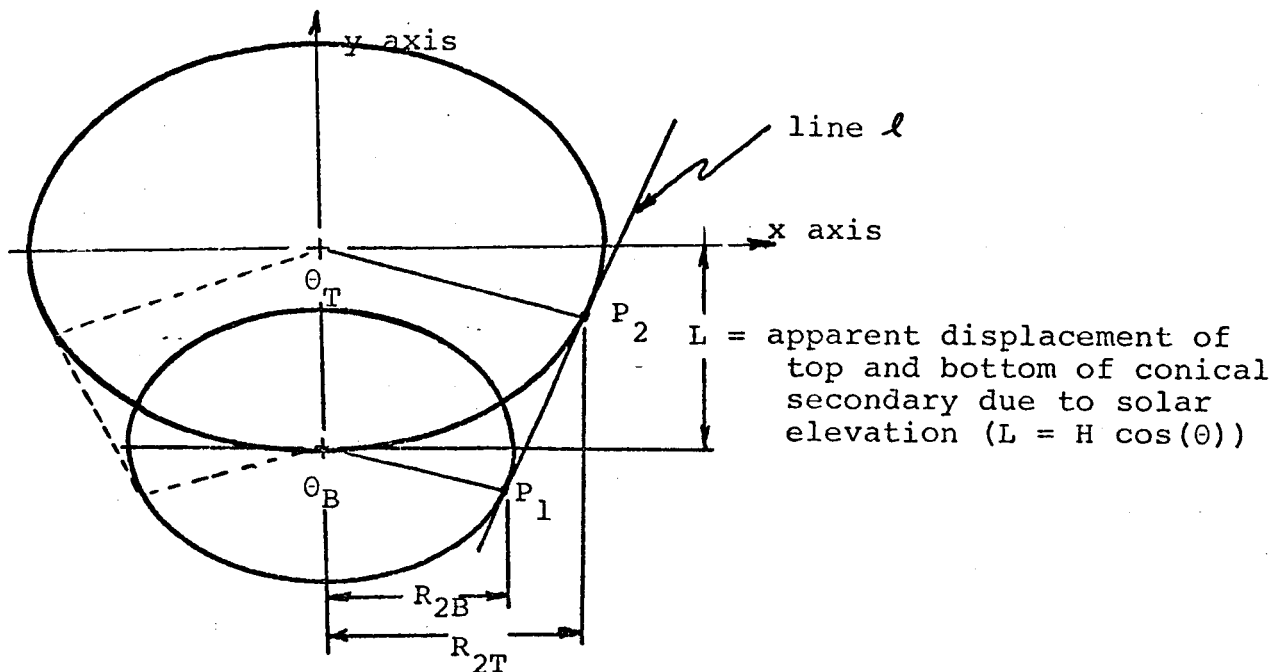


Figure B.4 - Effective Area Coordinate System

The calculation of A_{eff} may be simplified by breaking it into three segments, such that $A_{\text{eff}} = A_{\text{trap}} - A_{\text{seg t}} + A_{\text{seg b}}$ as shown in Figure B.5.

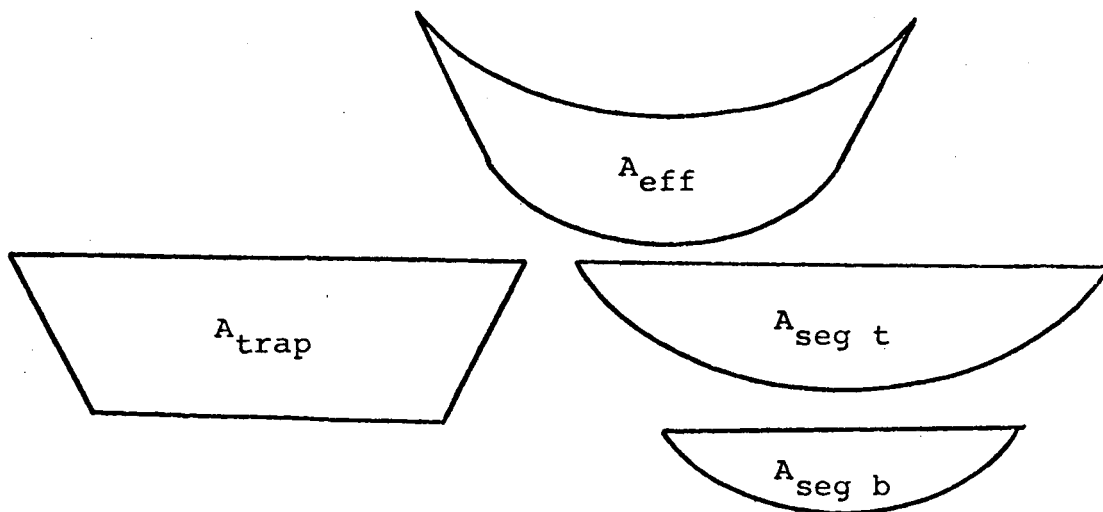


Figure B.5 - Breakdown of A_{eff} into Simpler Area

Calculation of A_{trap} , $A_{\text{seg t}}$, and A_{segb}

The top and bottom circular areas of a truncated cone appear as ellipses when viewed from an oblique angle. Referring to Figure B.4, the equations for top and bottom ellipses are as follows.

$$\frac{x^2}{l^2} + \frac{y^2}{\sin^2(\theta)} = R_{2T}^2 \quad (\text{top ellipse}) \quad (\text{B.1})$$

$$y = -\sin(\theta) \sqrt{R_{2T}^2 - x^2} \quad (\text{B.2})$$

(negative root to maintain consistency with Figure B.3; lower half of ellipse)

$$\frac{x^2}{l^2} + \frac{(y + L)^2}{\sin^2(\theta)} = R_{2B}^2 \quad (\text{bottom ellipse}) \quad (\text{B.3})$$

$$y = -L - \sin(\theta) \sqrt{R_{2B}^2 - x^2} \quad (\text{B.4})$$

(negative root for lower half of ellipse)

Implicit differentiation of equation B.1 yields

$$\frac{dy}{dx} = \frac{-2x \sin^2(\theta)}{2y} = \frac{x \sin(\theta)}{\sqrt{R_{2T}^2 - x^2}} \quad (\text{B.5})$$

The coordinates of points P_1 and P_2 in Figure B.4 are

$$P_2 \equiv (x, y) = (x, -\sin(\theta) \sqrt{R_{2t}^2 - x^2})$$

$$P_1 \equiv (x', y') = \left(x \frac{R_{2B}}{R_{2T}}, -L - \sin(\theta) \sqrt{R_{2B}^2 - \frac{R_{2B}^2}{R_{2T}^2} x^2} \right)$$

The slope of line ℓ and the slope of the ellipses in Figure B.4 must be equal at points P_1 and P_2 since line ℓ is tangent at these points.

$$\frac{dy}{dx} = \frac{y - y'}{x - x'} \quad (\text{B.6})$$

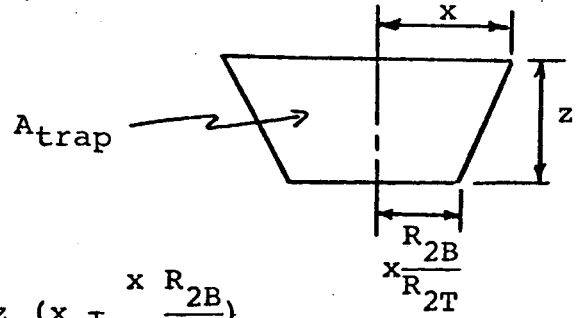
Equation B.6 may be solved for coordinates of P_2 in terms of R_{2B} , R_{2T} , θ , and H .

$$\frac{x \sin(\theta)}{\sqrt{R_{2T}^2 - x^2}} = \frac{-\sin(\theta) \sqrt{R_{2T}^2 - x^2} + L + \sin(\theta) \frac{R_{2B}}{R_{2T}} \sqrt{R_{2T}^2 - x^2}}{x - x \frac{R_{2B}}{R_{2T}}}$$

$$x = \frac{R_{2T} \sin(\theta)}{L} \sqrt{\frac{L^2}{\sin^2(\theta)} - R_{2B}^2 + 2R_{2B}R_{2T} - R_{2T}^2} \quad (\text{B.7})$$

where the positive root is taken for the right hand side of the ellipse, and $L = H \cos(\theta)$

The value of x may now be used to calculate the areas of the trapezoid and segments (see Figure B.5)



The diagram shows a trapezoid with a vertical height z . The top horizontal edge has a length x . The bottom horizontal edge has a length $R_{2B} + x \frac{R_{2B}}{R_{2T}}$. A dashed vertical line is drawn from the top edge to the bottom edge. An arrow labeled A_{trap} points to the trapezoid.

$$A_{\text{trap}} = z \cdot \left(x + \frac{x R_{2B}}{R_{2T}} \right) \quad (\text{B.8})$$

$$\text{where } z = (H \cos(\theta) - R_{2T} \cos(\frac{\theta}{2}) + R_{2B} \cos(\frac{\theta}{2}))$$

$$\text{and } \theta_T = 2 \sin^{-1}(x/R_{2T})$$

$$\theta_B = \theta_T \text{ since the ellipses are geometrically similar}$$

$$A_{\text{seg } t} = \sin(\theta) \left[\frac{\theta_T}{2} R_{2T}^2 - x \cos\left(\frac{\theta_T}{2}\right) R_{2T} \right] \quad (\text{B.9})$$

$$\text{for } R_{2T} \geq R_{2B}$$

$$A_{\text{seg } b} = \sin(\theta) \left[\frac{\theta_B}{2} R_{2B}^2 - x \frac{R_{2B}}{R_{2T}} \cos\left(\frac{\theta_B}{2}\right) R_{2B} \right] \quad (\text{B.10})$$

$$\text{for } R_{2T} \geq R_{2B}$$

Using equations B.8, B.9, and B.10, the effective absorbing area of a cone may be calculated as

$$A_{\text{eff}} = A_{\text{trap}} - A_{\text{seg } t} + A_{\text{seg } b} \quad (\text{B.11})$$

For determining A_{eff} of conical surface with $\beta > \frac{\pi}{2}$ the equations for $A_{\text{seg } t}$ and $A_{\text{seg } b}$ become

$$A_{\text{seg } t} = \sin(\theta) \left[\frac{(2\pi - \theta_T)}{2} R_{2T}^2 - x \cos\left(\frac{\theta_T}{2}\right) R_{2T} \right] \quad (\text{B.12})$$

$$\text{for } R_{2T} < R_{2B}$$

$$A_{\text{seg } b} = \sin(\theta) \left[\frac{(2\pi - \theta_B)}{2} R_{2B}^2 - \frac{R_{2B}}{R_{2T}} \cos\left(\frac{\theta_B}{2}\right) R_{2B} \right] \quad (\text{B.13})$$

$$\text{for } R_{2T} < R_{2B}$$

REFERENCES

1. Chapman, Alan J., Heat Transfer, MacMillan Co., New York, 1967.
2. Glaser, Black, and Lindstrom, Thermal Insulation Systems, A Survey, NASA SP-5027, 1967.
3. Hamilton and Morgan, Radiant-Interchange Configuration Factors, NACA TN 2836, December 1952.
4. Krieth, Frank, Radiation Heat Transfer, for Spacecraft and Solar Power Plant Design, International Textbook Company, USA, 1962.
5. Surveyor III, A Preliminary Report, NASA SP-146, June 1967.